A T-resonator Technique for Aperture Plane Admittance Parameters of Electrically Short RF Monopoles

Phumezo M. Kwinana

Thesis presented in fulfillment of the Master of Science in Engineering at the University of Stellenbosch.

Supervisor: Prof. Johannes H. Cloete

December 2006

Declaration

I, the undersigned, hereby declare that the work contained in this thesis is my own original work, unless otherwise stated, and that I have not previously, in its entirety or in part, submitted it at any university for a degree.

_____

Phumezo Mzoxolo Kwinana Date: November 2006

Summary

This thesis focuses on the coaxial-microstrip T-resonator measurement technique to determine the aperture plane capacitance and radiation resistance of electrically short monopoles above a finite ground plane at Radio Frequencies. The determination of these impedance parameters is of interest as they are needed in the Thévenin equivalent circuit of the monopole to establish the relationship between the monopole, the electromagnetic field within which it is immersed, and its surrounding medium properties. Electromagnetically short monopoles are used in various applications such as in permittivity and biomedical measurement techniques and near-field metrology.

The coaxial-microstrip device allows the measurement of transmission coefficient nulls when connected to the network analyser. By measuring the frequency shift in transmission null points and analysing the results, the capacitance of short monopoles of various lengths can be obtained. The radiation resistance of the monopole can also be determined by comparing the depth of transmission coefficient nulls points at various resonant frequencies.

Monopoles ranging from flush-mounted to various sizes of protruding centre conductors, both bare and insulated, are investigated in the frequencies ranging from 45 MHz to 3 GHz. The experimental results compare well with FEKO numerical predictions at the ranges where this technique is applicable. The technique is however not applicable near and beyond the resonant frequency of the monopole where it is considered to be electrically long.

Measurements to obtain monopole impedance parameters were conducted by connecting the device to the HP 8510C Network Analyser. To enhance accuracy, the Network Analyser was calibrated using a high quality calibration kit with precisely defined standards. The technique used was found to accurately yield capacitances in the range of 0.0211 to 1 pF and radiation resistances in the range of 0.9245 to 12.1 Ohms. These results were obtained for monopoles of length $0.0062 < h/\lambda < 0.24$. Results from literature, viz. W.R Scott, R.W.P. King and L.J. Cooper, show radiation resistance in the ranges: 2.5 to 35 Ohms ($0.079 < h/\lambda < 0.22$), 1.26 to 74.08 Ohms

(0.026 < h/λ < 0.28) and 5.59 to 74.98 Ohms (0.1 < 0.28) for electrically short monopoles. The results of this work are compared with those in the literature and show variations of less than 6%.

A technique capable of accurately measuring capacitance and radiation resistance of the monopole at various lengths of protruding centre conductor has been developed. The capacitance for a flush probe compares very well (agreement is less than 6%) when compared with those obtained by the previous researchers. The technique is capable of yielding accurate results radio frequencies in the challenging low radiation resistance range around 1 Ohm.

Opsomming

Die fokus van hierdie tesis is die koaksiale-mikrostrook T-resonator meet-tegniek wat gebruik word by radio frekwensies om die vlak kapasitansie enstralingsweerstand van elektries kort monopole bo ’n eindige grondvlak te bepaal. Die bepaling van hierdie impedansie parameters is van belang aangesien dit benodig word in die Thévenin ekwivalente baan van die monopool om die verwantskap tussen die monopool, die elektromagnetiese veld waarin dit gedompel is, en die eienskappe van die omliggende medium te bepaal. Elektromagneties kort monopole word gebruik in verskeie aanwendings, soos permittiwiteit en biomediese meet-tegnieke en naby-veld metrologie.

Die koaksiale-mikrostrook apparaat laat toe die transmissie koëffisiënt wanneer dit aan die network analiseerder gekoppel is. Deur die frekwensie verskuiwing in transmissie nul-punte te meet en te analiseer, is dit moontlik om die kapasitansie van kort monopole van verskeie lengtes te bepaal. Deur die diepte van die transmissie koëffisiënt nul-punte teen verskillende resonante frekwensies te vergelyk, is dit ook moontlik om die stralingsweerstand van die monopool te bepaal.

Monopole met geleiers arverskillende die senter geleier lengte s, beide onbedek sowel as geïsoleerd, word ondersoek in die frekwensies bereik vanaf 45 MHz tot 3 GHz. Die eksperimentele resultate vergelyk goed met die numeriese voorspellings van FEKO binne die perke waar hierdie tegniek toepasbaar is. Dit is egter nie moontlik om hierdie tegniek toe te pas naby of verby die resonante frekwensie van die monopool waar dit as elektries lank beskou word nie.

Metings met die doel om monopool impedansie parameters te verkry is uitgevoer deur die apparaat aan ’n HP 8510C Netwerk Analiseerder te koppel. Om akkuraatheid te verbeter is die Netwerk Analiseerder gekalibreer deur die gebruik van ’n hoë-kwaliteit kalibrasie-stel met goed gedefinieerde standaarde. Die tegniek wat ontwikkel is het akkurate kapasitansies gelewer vanaf 0.0211 tot 1 pF en stralingsweerstand vanaf 0.9245 tot 12.1 Ohm. Hierdie resultate is verkry vir die lengtes oor die bereik $0.0062 < h/\lambda < 0.24$. Ander navorsers, by name W.R Scott, R.W.P. King en L.J. Cooper het

stralingsweerstand in die volgende bereik gemeet: 2.5 tot 35 Ohm ($0.079 < h/\lambda < 0.22$), 1.26 tot 74.08 Ohm ($0.026 < h/\lambda < 0.28$) en 5.59 tot 74.98 Ohm ($0.1 < 0.28$) vir elektries kort monopole. Die resultate van hierdie werk vergelyk goed met resultate, met ’n afwyking van minder as 6%.

’n Tegniek is ontwikkel wat kapasitansie en stralingsweerstand van ’n monopool akkuraat kan meet. tegniek lewer by radio frekwensies goeie meetresultate vir die uitdagende lae stralingsweerstand in die 1 Ohm bereik

Acknowledgements

I would like to sincerely thank Professor Johannes Cloete for his motivation and support through out this work. His invaluable contribution in terms of supervision, support and guidance is greatly appreciated.

I also would like to thank the National Research Foundation (NRF), the University of Fort Hare and the University of Stellenbosch for their financial support throughout this research work. Their support has afforded me an opportunity to improve my research capacity.

Many thanks to the staff at Central Electronic Services, especially Mr. Wessel Croukamp and Ulrich Butner for their careful work in constructing the measurement devices for this work. Their experience, technical skills, and advices are highly appreciated.

A special thanks to Marc Rütschlin for providing FEKO numerical data for this work.

I also would like to thank Professor Howard Reader for his guidance and useful ideas in enabling me to perform accurate measurements in the HP 8510C Network Analyser.

Finally, I would like to thank my late parents for their role they played to be the person I am today. I also would like to thank my family for their encouragement and support. A special thanks to my wife Ntombekhaya and my children Zuqhame and Khazimla, for their encouragement, time, motivation, support and confidence in me.

Contents

List of Figures

List of Tables

Chapter 1

Introduction

This thesis is concerned with the determination of the admittance parameters of electrically short monopoles at Radio Frequencies (RF) using a coaxial-microstrip T-resonator technique. Coaxial monopoles have found numerous applications in fields such as permittivity, biomedical and electric-field measurement techniques. For accurate sensing of the near-field at point in a measurement space, the admittance parameters of the monopoles have to be determined with high precision as they play an important role, both as receiver and as source, in establishing the relationship between the monopole, the electromagnetic field within which it is immersed, and its surrounding medium properties.

1.1 Research Challenge

As discussed in Section 1.2 of this chapter, extensive research has been done in determining admittance parameters of electrically short monopoles. However, further research is still needed to develop alternative experimental techniques that will accurately yield radiation resistance of electrically short monopoles even below 1 Ohm and sub-pico Farad capacitances in low ranges (e.g. 0.01pF to 1pF). Kraszewski and Stuchly [8] used the T-resonator technique to accurately measure capacitance of flush open-ended coaxial lines. Their emphasis was on monopole reactance. The advantage of their work was to measure frequency with precision. Though their work produced good results with 95% confidence for flush-mounted monopoles, they did not explicitly explain the theory and did not show any possibilities of extending the method to measure the radiation resistance of the monopole.

A recent attempt to use the experimental technique to measure monopole reactance up to the flush transition point of the coaxial line (see Africon paper in Appendix A) based on the inversion of the measured reflection coefficient at the monopole's input port is reported. The method is limited by the fact that phase constant is sensitive to small perturbations in input reflection coefficient measurements. It is hence not

applicable when the centre conductor of an open-ended coaxial line is very short and when it is flush in its aperture plane. It is also not suitable for measuring radiation resistance of the electrical short monopoles in RF.

Previous researchers in this field also made attempts to experimentally determine admittance parameters of electrically short monopoles. W.R. Scott [9] measured the complex dielectric permittivity of a material over a broad range (50 MHz to 18 GHz) using a monopole antenna. The antenna was calibrated firstly by measuring the input admittance in a standard medium with known permittivity and secondly when the antenna was immersed in a material with unknown permittivity. The comparison was then used to obtain the permittivity of the material. The advantage of his method is that it could measure input impedance over a broad range of frequencies and the reactance results compared very well with the finite-difference time-domain (FDTD) numerical calculations by J.G. Maloney [11, Fig 9]. The disadvantage of his method is that it could not measure the radiation resistance of the short monopole below 2.5 Ohms in the range $0.079 < h/\lambda < 0.6$.

L.J. Cooper [6] measured in the range: $0.0625 < h/\lambda < 0.4$ for a range of lengths surrounding the first resonance of the monopole antenna and estimated the error bound on his measurement data to be 5%. His method also compares very well with the finite-difference time-domain (FDTD) numerical calculations of J.G. Maloney [11] but it could not measure radiation resistance below 5.5 Ohms in the indicated range. R.S. Elliott [5] tabulated impedance of thin monopoles over a large ground plane where entries of his data were calculated by linear interpolation and inversion of data by King [4]. The impedance was obtained in the range: $0.0625 < h/\lambda < 0.375$.

The developed T-resonator technique in this thesis is good for $0.0062 < h/\lambda < 0.2338$. The comparison of the measurement results of the above-mentioned investigators with this technique is represented graphically in Fig. 1.1 below. The T-resonator technique accurately yields capacitances in the range 0.0211 pF to 1 pF and is suitable for both flush and extended centre conductors of the coaxial lines. It is also applicable for the measurements of the radiation resistance at Radio Frequencies in the range 0.9245 to 12 Ohms. A recent paper (See Appendix B) shows that the T-resonator method

compares well with numerical predictions by FEKO [13] below the resonant frequency of the monopole. It is, however, not applicable near and beyond the resonant frequency of the monopole where it is electrically long. As can be seen in Fig. 1.1 below (detailed analysis in Chapter 3), the T-resonator technique is capable of measuring the radiation resistance at very low h/λ and can measure radiation resistance up to as low as 1 Ohm. The results compare well with numerical predictions and when compared with previous researchers.

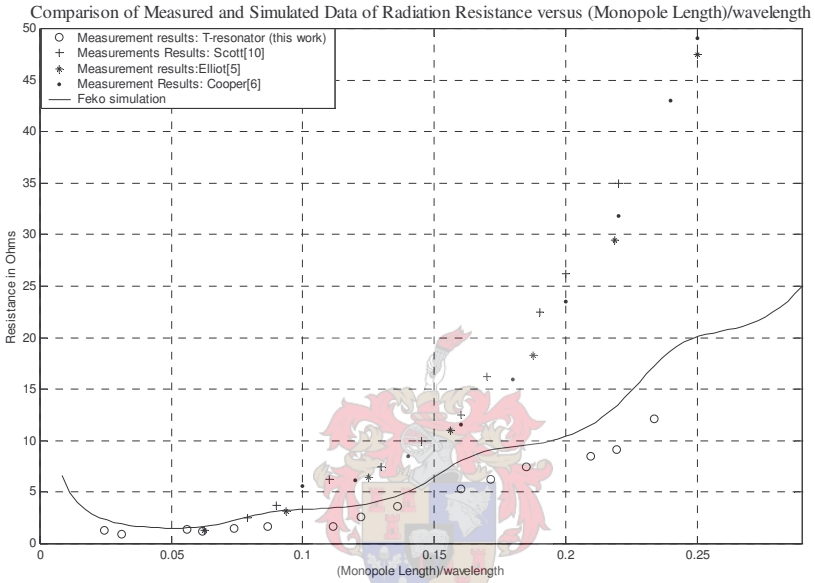

Figure 1.1 A graphical representation of measured data for the radiation resistance determined by the T-resonator technique of this thesis along with other published results

1.2 Literature Review

Analytical and experimental techniques on coaxial monopoles have been advancing for decades. Levine and Papas developed the theoretical analysis of the aperture admittance parameters of the coaxial line using the variation method [1]. In 1951, Marcuvitz developed a model for the computation of coaxial line aperture admittance parameters [2]. The theory was further developed by Galejs to cater for higher order modes [3]. In 1971, King published data on the input admittance for monopoles of various sizes [4]. In the early eighties, R.S Elliott [5] used King's data to calculate impedance of thin monopoles over a big ground plane by linear interpolation and inversion of the data. In 1975, L.J. Cooper measured admittance parameters of monopoles on electrically thick conducting cylinders [6]. His measurement results

compared well with the Finite-Difference Time-Domain (FDTD) numerical predictions.

In 1983, Gajda and Stuchly used Finite Element Method (FEM) and Methods of Moments (MOM) numerical predictions to determine the capacitance of the flush coaxial monopole [7]. Krazewski and Stuchly later verified these numerical results using the T-resonator experimental technique [8]. W.R. Scott measured complex dielectric permittivity using monopole antennas of general length [9]. In 1990, Maloney *et al.* [11, Fig. 9] used FDTD numerical predictions to compare measured results by W.R. Scott with good agreement. Misra developed the theoretical analysis based on the approximate evaluation of the integrals for the determination of the coaxial monopole admittance [10].

Recently, Smith *et al.* [12] further analysed monopoles using finite-difference time-domain (FD-TD) with good agreement when compared with experimental data of Cooper and Scott. In a recent paper (See Appendix B), The T-resonator method has been extended to measure both reactance and radiation resistance of the electrically short monopoles.

This thesis presents research based on the T-resonator experimental technique to determine the impedance parameters with special emphasis on the radiation resistance of electrically short coaxial probes at radio frequencies. Measurements were taken using HP 8510C network analyser in the frequency range from 45 MHz to 3 GHz. The experimental results compare well with the numerical predictions using FEKO [13] simulation technique. Both bare and insulated monopoles are studied. The T-resonator technique was also used by Peterson *et al.* to characterize microwave substrates [14].

1.3 Summary of the T-resonator Experimental Technique

The analytical model developed by Krazewski and Stuchly [8] conveys the key idea in determining the aperture capacitance of the flush mounted monopole. In this thesis, a rigorous analytical approach to determine equations for computing both capacitance

and radiation resistance of electrically short monopoles is developed. The equations are then used to analyse experimental observations. Consider the one-port coupling model used to obtain experimental results for this work shown in Fig. 2 below.

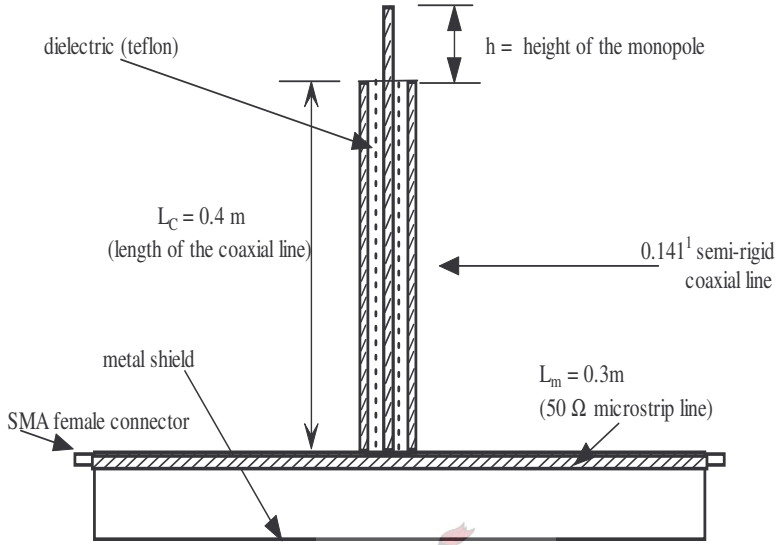

Fig. 1.2 Cross-section of the one port model of the micro-strip-coaxial coupling device

The coaxial line that shunts the micro-strip line is either open or short-circuited at its output end. When the coupling device is connected to the network analyser, energy is transmitted through from one port to the other and some goes to the coaxial line that shunts the shielded micro-strip line. When, for example, the coaxial line is either open- or short-circuited at its output end, the line transforms to a shunt short circuit on the micro-strip line at all odd or even quarter-wave lengths. The electrical length of the coaxial line can be precisely determined from the transmission null frequencies.

By measuring the frequency shift in transmission coefficient null points, the capacitance of the monopoles of various lengths, including the flush case, can be obtained. Also, by comparing the depth of the transmission coefficient null points of shielded and unshielded monopoles at various resonant points, the radiation resistance of the monopoles can be determined. The method is applicable for both the flush and extended centre conductor cases. The experimental results are compared with numerical predictions and research work by previous authors. Both bare and insulated monopoles were studied.

All measurements were done using the HP 8510C network analyser. To enhance accuracy, the network analyser was first calibrated using high quality calibration kit. A T-resonator measurement system, as described above, was used to obtain resonance measurements in the frequency range of 45 MHz to 3 GHz. Measurements for the unshielded probes were performed in the anechoic chamber to minimize obstacle and room reflections.

The applicability of this technique is limited as explained in Section1.1. Further work to experimentally verify the coaxial monopole by predicting and measuring the signal delivered to a spectrum analyzer when a monopole is inserted in a known electromagnetic field is suggested.

1.4 Contribution

The contributions of this work are the following:

(i) Extension of the T-resonator technique by Kraszewski and Stuchly [8] on formulating an analytical model to accurately measure capacitance of electrically short monopoles for both flush and extended centre conductor cases at Radio Frequencies.

(ii) The development of an analytical model to compute the monopole radiation resistance of electrically short monopole applicable for both flush and extended centre conductor cases.

(iii) The development of a T-resonator measurement technique to measure the radiation resistance of the electrically short monopoles, both bare and insulated, at Radio Frequencies.

Chapter 2

Measurement of the Reactance of Electrically Short Monopoles at Radio Frequencies Using a T-resonator Technique

An experimental technique to accurately determine reactance parameters of electrically short monopoles using a T-resonator technique is presented. The technique is based on the idea provided by Kraszewuski and Stuchly [8]. In this chapter, a rigorous analytical model to accurately measure capacitance of electrically short monopoles, both flush and extended centre conductor cases at Radio Frequencies, is presented. Measurements were taken using an HP 8510C network analyser in the frequency range 45 MHz to 3 GHz. By measuring the frequency shift in transmission coefficient null points, the capacitance of the monopoles of various lengths can be obtained. The method is applicable for both the flush and the extended centre conductor cases. The experimental results are compared with numerical predictions. Both bare and insulated monopoles were studied.

2.1 Derivation of the Equation to Compute Coaxial Monopole Capacitance

Consider the one port model of the microstrip-coaxial coupling device as shown in Fig. 1.2 in Chapter 1. Its equivalent circuit is shown below in Fig. 2.1. The coupling device consists of a 50Ω semi-rigid coaxial line (0.141″) that shunts the shielded 50Ω microstrip line. The microstrip line is terminated in its characteristic impedance and has SMA female connectors at both ends. The coaxial line is either open- or short-circuited at its output end.

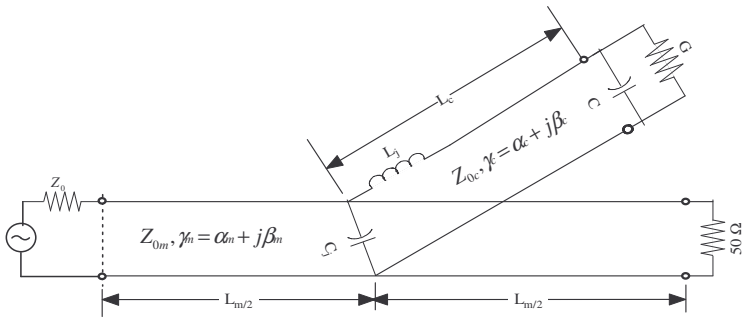

Fig. 2.1 One port model of the microstrip-coaxial coupling device for the open-circuited coaxial line, or with electrically short monopole at the output end

The coaxial line model that shunts the micro-strip line in cases when it is open and short-circuited is shown in Fig. 2.2 below:

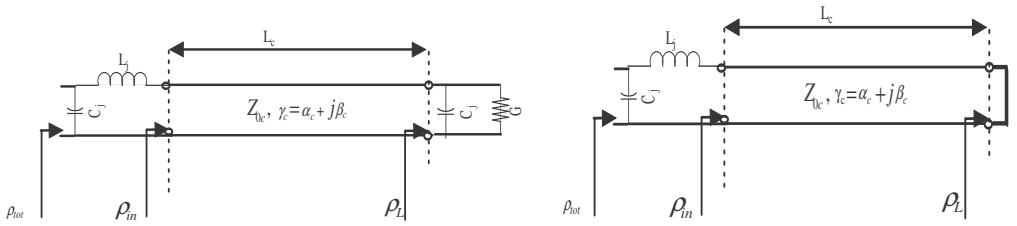

(a) (b)

Fig. 2.2 (a) Open-circuited coaxial line model that shunts the microstrip line (b) Short-circuited coaxial line model that shunts the microstrip line (L_j and C_j represent junction effects).

From the transmission line theory [15] and with reference to the terms in Fig. 2.2, it can be shown that for the radiating open-circuited coaxial line, the input reflection coefficient of the coaxial line is given by

$$\rho_{in} = p_L \exp\left\{-2\left(\alpha_c L_c\right) - 2j\omega\left(\frac{L_c}{v_c}\right)\right\} \tag{2.1}$$

$$\rho_L = \exp\{-2\alpha_G - j2\phi_c\} \tag{2.2}$$

where, $\alpha_G = G\,Z_{0C} << 1$ and $\phi_C = \omega C Z_{0C} << 1$ for the radiating open-circuited coaxial line. G and C are the radiation conductance and capacitance at the aperture plane of the coaxial line. Z_{0C} is the characteristic impedance of the coaxial line and ω is the angular frequency. L_c and v_c are length and phase velocity of the coaxial line. On substituting Eq. 2.2 into Eq. 2.1, we get

$$\rho_{in} = \exp\left\{-2(\alpha_G + \alpha_c L_c) - 2j\left(\phi_c + \omega\left(\frac{L_c}{v_c}\right)\right)\right\} \tag{2.3}$$

From Eq. 2.3, if we let $\phi_{in} = -2(\phi_c + \omega(\frac{L_c}{v_c}))$ (2.4)

then $-\phi_{in} = 2\omega(CZ_{0c} + (L_c/v_C))$ (2.5)

It can be shown that

$$-\phi_{in} = n\pi = 2\omega_{r,n}\,(CZ_{0c} + (L_c/v_c)) \qquad (2.6)$$

where $\omega_{r,n}$ is the angular frequency for each corresponding odd quarter wave length and n (resonance index) = 1, 3, 5, … and r indicates resonance. To illustrate how L_c can be obtained at various resonance points, let us consider the example below:

Example 2.1: When C = 0 (assuming perfect open) and $\rho_L = 1$ at first resonance point (i.e. at n = 1), Eq. 2.6 becomes

$$\omega_{r,1} = \frac{\pi}{2}\left(\frac{v_c}{L_c}\right) = 2\pi f_{r,1} \qquad (2.7)$$

$$\therefore\ L_c = \lambda_{r,1}/4 \qquad (2.8)$$

In general, Eq. 2.6 can be written as

$$CZ_{0c} + \frac{L_c}{v_c} = \frac{n}{4f_{r,n}} \qquad (2.9)$$

L_c/v_c is quantified by short-circuiting the coaxial line at its output end (i.e. assuming "perfect" short) as shown in Fig 2.2 (b) above and measuring frequencies at even quarter wavelength multiples. At all even quarter wave resonant points, L_c transforms into:

$$L_c = \frac{(n+1)}{4}\lambda_{r,n+1},\ \text{n odd.} \qquad (2.10)$$

Where $\lambda_{r,n+1} = v_c/f_{r,n+1}$ is the wavelength at all even quarter-wave points. On rearranging Eq. 2.10, L_c/v_c is hence given by:

$$\frac{L_c}{v_c} = \frac{(n+1)}{4} f_{r,n+1} \qquad (2.11)$$

on combining Eqs. 2.9 and 2.11, rearranging and generalizing, it can be shown that the final equation to compute the capacitance of the monopoles is given by

$$C = \frac{1}{4Z_{0c}}\left(\frac{n}{f_{r,n}} - \frac{n+1}{f_{r,n+1}}\right), \; n \text{ odd.} \tag{2.12}$$

Thus, the capacitance can be precisely measured by determining the shift of frequency in Eq. 2.12 above. To illustrate the practicability of Eq. 2.12 above, consider the Example below:

Example 2.2: Suppose we use Eq. 2.12 to examine whether it is possible to obtain $f_{r,1}$ given the capacitance value obtained by Kraszewuski and Stuchly [8] (i.e. 0.022pF for a flush probe) at say, $f_{r,2}$ = 1000 MHz, for a 0.141˝ semi-rigid coaxial line.

Firstly, on rearranging Eq. 2.12 to

$$CZ_{0c} = \frac{1}{4f_{r,1}} - \frac{1}{2f_{r,2}} = \frac{(f_{r,2} - 2f_{r,1})}{4f_{r,1}f_{r,2}}, \tag{2.13}$$

as would be expected for a shorted line. It is found that for C = 0,

$$f_{r,1\_0} = \frac{1}{2} f_{r,2} \tag{2.14}$$

Secondly, define $f_{r,1}$ as $f_{r,1} = f_{r,1\_0} + \Delta f_{r,1}$ (2.15)

On rearranging Eqs. 2.15 and 2.13, it can be shown that

$$\Delta f_{r,1} = -4CZ_{0c} f^{2}{}_{r,1\_0} \tag{2.16}$$

By substituting the given quantities, it can be shown that $f_{r,1\_0}$ = 500 MHz and that the shift from $f_{r,1\_0}$ is -1.1 MHz, a measurable value using the HP 8510C.

2.2 Extension of Equation 2.12 to Cater for Junction Parameters of the Coupling Device

Equation 2.12 was derived assuming that there were no junction effects (i.e. Cj = Lj ≈0). An investigation to examine the possible junction effects was carried out by analysing the equivalent circuit of the coaxial line with junction parameters. Consider the equivalent circuit of the coaxial resonator with junction parameters as shown below:

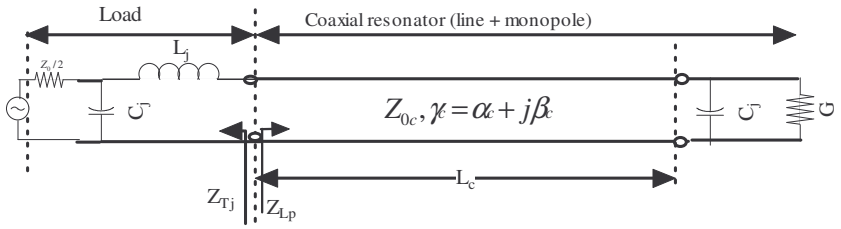

Fig. 2.3 Equivalent circuit of the coaxial resonator with junction parameters

From the Fig. 2.3, Z_{Tj} and Z_{Lp} represent the impedance of the load and the coaxial resonator from the junction. It can be shown that Z_{Tj} and Z_{Lp} for a short-circuited coaxial line are given by:

$$Z_{Lp} \cong R_s + j2L_s(\omega - \omega_0), \tag{2.17}$$

with $Rs = \alpha_c + L_c Z_{0c}$ and $Ls = (\pi/2)(Z_{0c}/\omega_0)$, $(\omega - \omega_0) = \Delta\omega$ and

$$Z_{Tj} \cong Z_{0c}/2 + j\omega(dX(\omega)/d\omega) \tag{2.18}$$

with $\omega = \omega_0 + \Delta\omega$ and $(dX(\omega)/d\omega) = Lj - (Cj\ (Z_0^2)/4)$. At resonance, the sum of the imaginary parts of Eqs. 2.17 and 2.18 must add up to zero. That is,

$X_{Tj} + X_{Lp} = 0$ (at resonance, equilibrium of stored electrical and magnetic energy equals to zero [15, Chap. 11, p562]) (2.19)

On rearranging Eq. 2.19 and solving, it can be shown that the reactance slope for a short-circuited coaxial line is computed using the following equation:

$$\frac{\Delta f_{n+1}}{f_{r,n+1\_0}} = \frac{-(4f_{r,n+1\_0}X'_{short})/((n+1)Z_0)}{1+(4f_{r,n+1\_0}X'_{short})/((n+1)Z_0)}, \text{ n odd} \quad (2.20)$$

where $\Delta f_{n+1} = f_{r,n+1} - f_{r,n+1\_0}$ and $f_{r,n+1\_0}$ is the theoretical resonance frequency for a short-circuited line and X'_{short} is the reactance slope. Similarly, it can be shown that the general equation to compute the reactance slope for an open-circuited coaxial line is given by:

$$\frac{\Delta f_{n}}{f_{r,n\_0}} = \frac{-(4f_{r,n\_0}X'_{open})/((n)Z_0)}{1+(4f_{r,n\_0}X'_{open})/((n)Z_0)}, \text{ n odd} \quad (2.21)$$

where $\Delta f_n = f_{r,n} - f_{r,n\_0}$ and f_{r,n_0} is the theoretical resonance frequency for an open-circuited line and X'_{open} is the reactance slope. Having derived Eq.s 2.20 and 2.21, Eq. 2.12 can then be modified to cater for the possible errors due to junction effects. Eq. 2.12 therefore becomes:

$$C = (1/(4Z0))((n/f_{r,nopen}) - ((n+1)/(f_{r,nshort+1}))), \text{ n odd} \quad (2.22)$$

where $f_{r,nopen}$ and $f_{r,nshort}$ are given by: $f_{r,nopen} = f_{r,n\_0} - \Delta f_n$ and $f_{r,nshort} = f_{r,n+1\_0} - \Delta f_{n+1}$.

2.3 Experimental Procedure

Having established the theoretical principles to measure the aperture capacitance and radiation resistance, the experimental procedures necessary to obtain reliable measurements are now described.

2.3.1 Experimental set up

All measurements were done using the HP 8510C network analyser. To enhance accuracy, the network analyser was first calibrated using a high quality calibration kit. A T-resonator measurement system as described in Section 2.1 above was used to obtain resonance measurements in the frequency range of 45 MHz to 3 GHz.

Measurements for the unshielded probes were performed in the anechoic chamber to minimize obstacle and room reflections. The ground plane was tightly fitted level to the coaxial line aperture plane. The sequence (i) to (iv) in Fig. 2.4 (a) describes the step-by-step procedure of mounting the measurement systems. The measurements for the shielded probes were done as described in Fig. 2.4 (b) below. The cylindrical shield [16] was designed to reduce radiation effects of the coaxial probe while causing negligible disturbance to the reactive near-fields that are dominant in the region.

The semi-rigid cable formed a monopole by extending its centre conductor by up to 40 mm beyond the coaxial aperture plane. The monopoles were then cut in steps up to the flush transition point and measurements were taken for each case. For the 40 mm, 20 mm, and 10 mm monopoles, measurements were done for two different cases:

(i) when the copper screen is removed, leaving the dielectric and extended centre conductor (insulated monopole) and

(ii) when the copper screen and the dielectric are removed, leaving the extended centre conductor in air (bare monopole).

Tables detailing the measurement values for different sizes of measured monopoles are illustrated in Appendix C. In the case of the 2.5 mm and the flush probes, both the copper screen and the dielectric were removed (i.e. no measurements for insulated monopoles were taken). The characteristic impedances and attenuation constants for both the microstrip and the coaxial line were experimentally determined using the HP 8510C network analyser. Details of their experimental procedure are in appendix D.

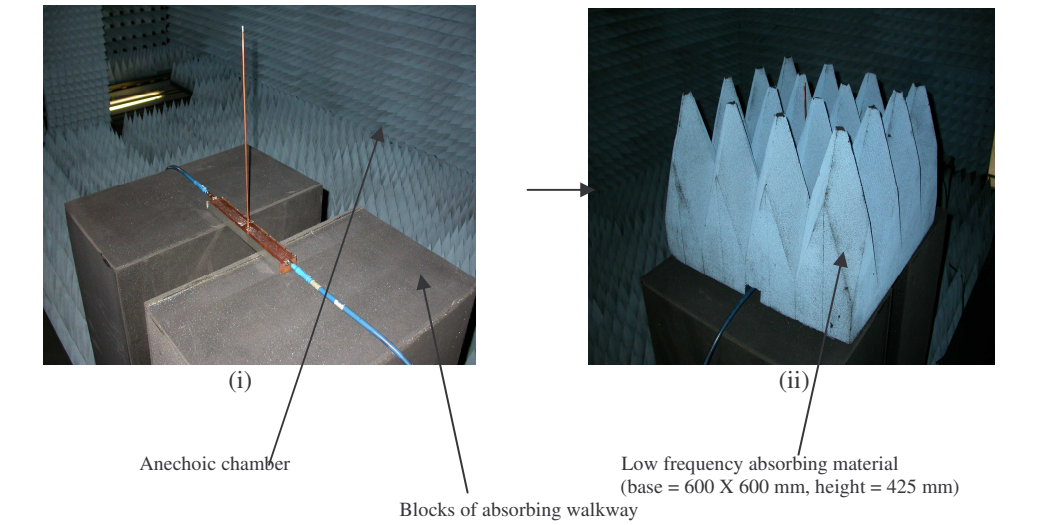

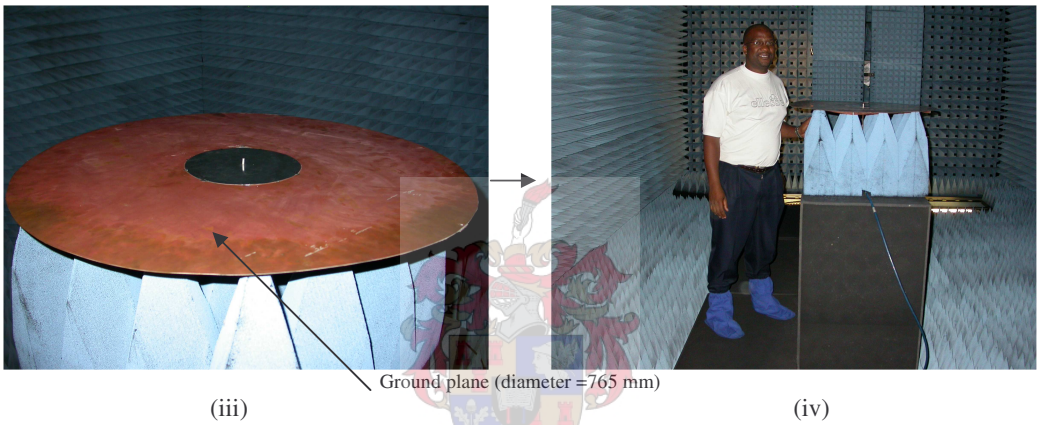

Fig. 2.4 (a) Procedure for mounting the microstrip-coaxial coupling device in the anechoic chamber

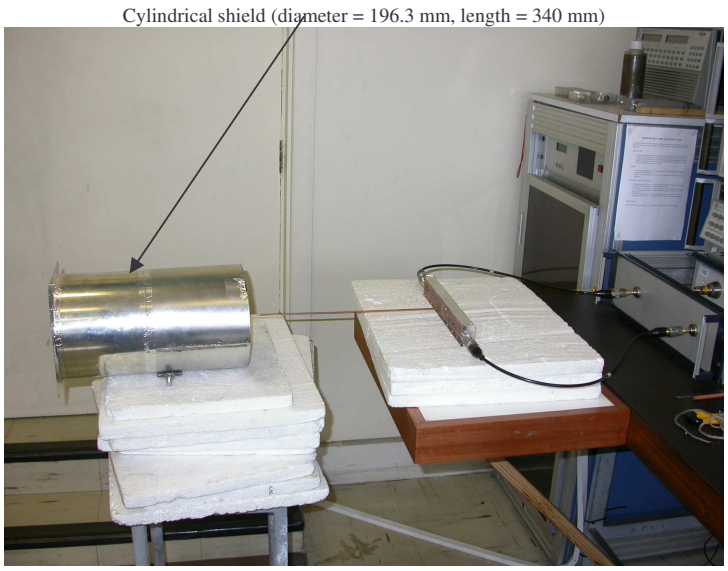

Fig. 2.4 (b) Measurement procedure for the shielded probes using HP 8510C Network Analyser

2.3.2 Results

Figures 2.5 to 2.12 show S_{21}(dB) measurements of the of unshielded and shielded monopoles (i.e. monopoles of sizes: 40 mm, 20 mm, 10 mm, 2.5 mm, and flush) using the coupling device described in Fig. 2.1. To enhance accuracy, the resolution around each quarter wave resonant point was improved to establish the exact tuning point. Note however that the numerical values given in Appendix C provide the quantitative data which were used to compute the monopole capacitances.

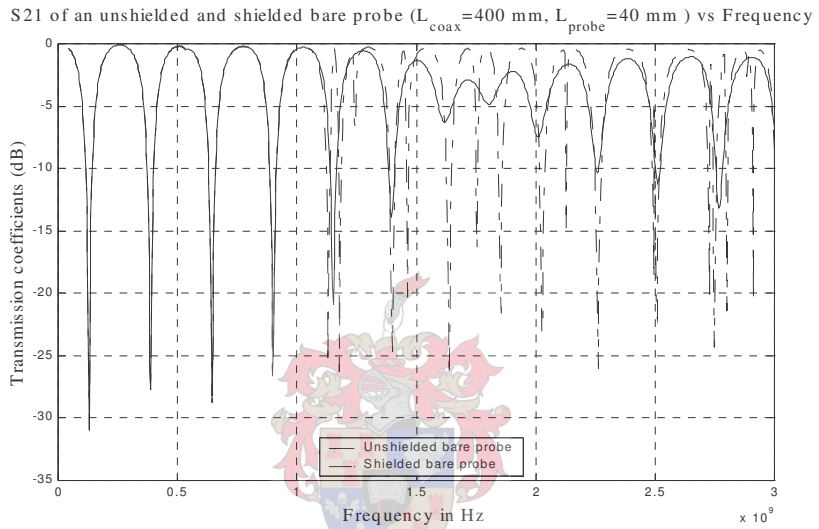

Fig. 2.5 S_{21} (dB) measurement results of the 40 mm unshielded and shielded bare monopole

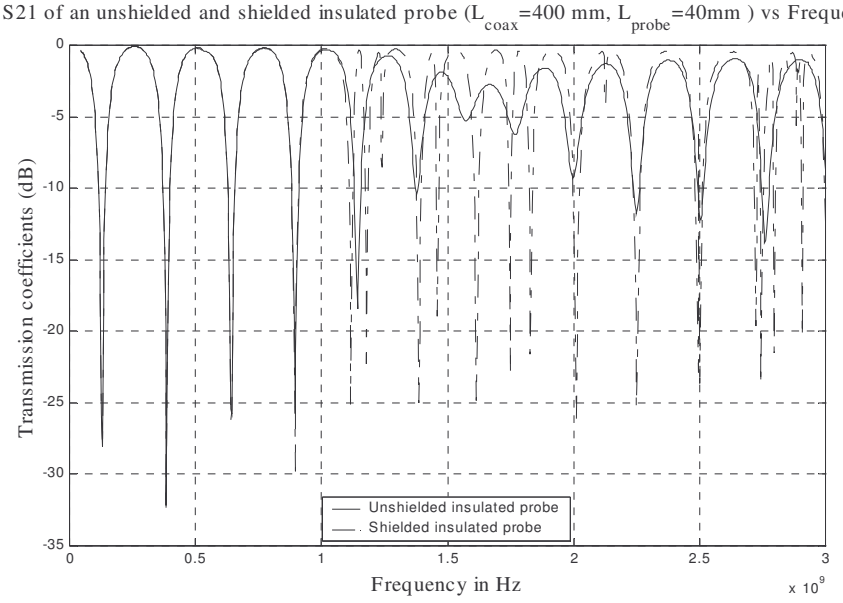

Fig. 2.6 S_{21} (dB) measurement results of the 40 mm unshielded and shielded insulated monopole

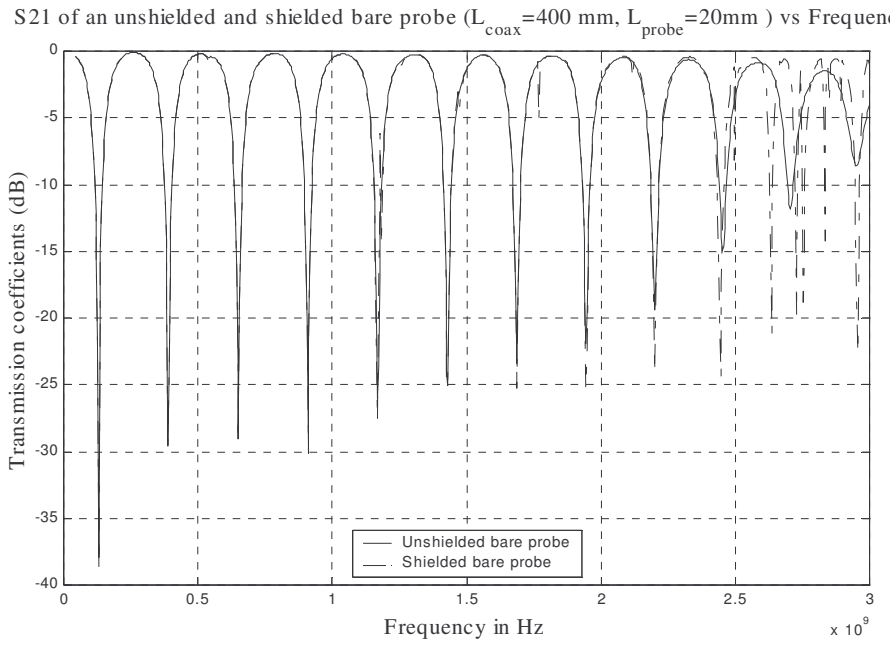

Fig. 2.7 S_{21} (dB) measurement results of the 20 mm unshielded and shielded bare monopole

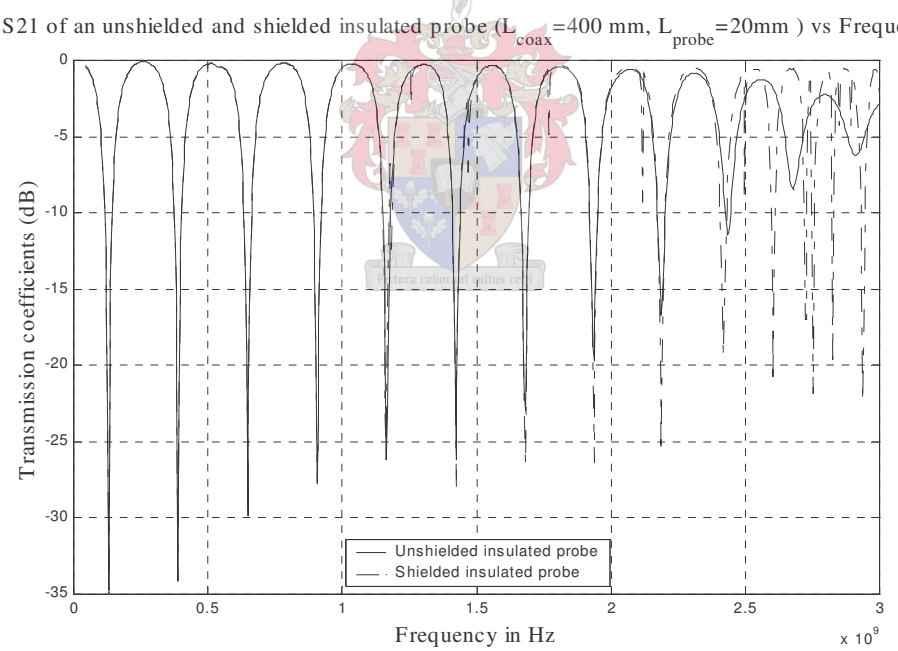

Fig. 2.8 S_{21} (dB) measurement results of the 20 mm unshielded and shielded insulated monopole

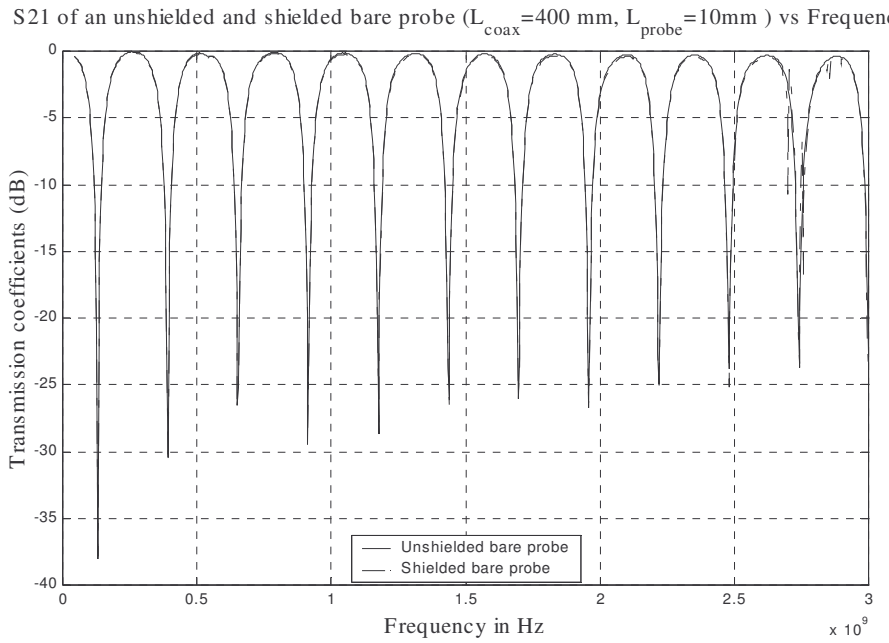

Fig. 2.9 S_{21} (dB) measurement results of the 10 mm unshielded and shielded bare monopole

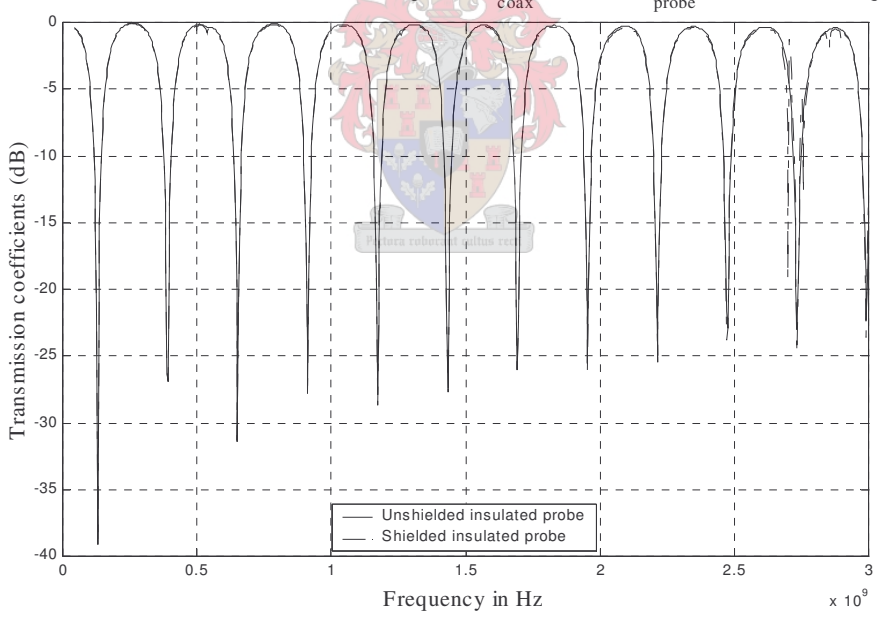

Fig. 2.10 S_{21} (dB) measurement results of the 10 mm unshielded and shielded insulated monopole

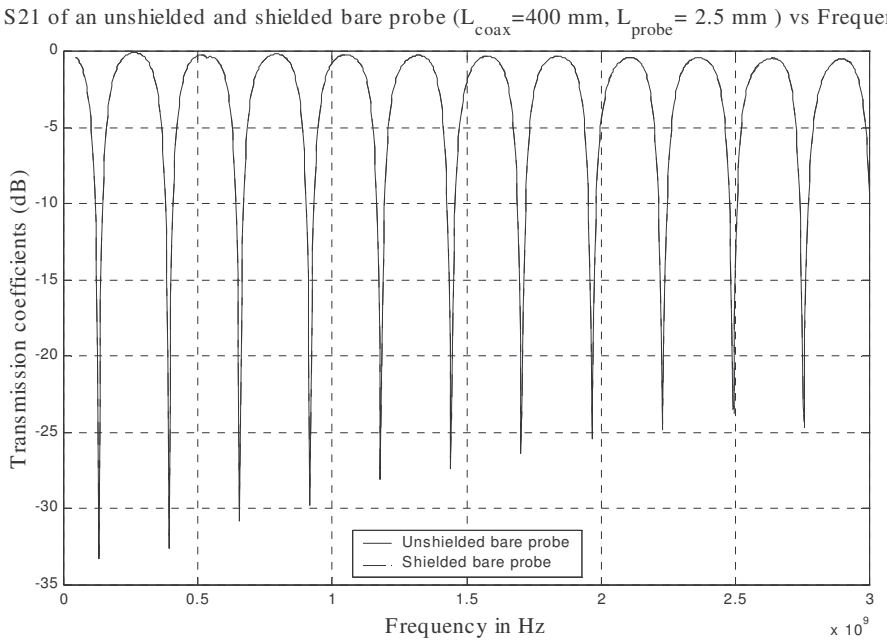

Fig. 2.11 S_{21} (dB) measurement results of the 2.5 mm unshielded and shielded bare monopole

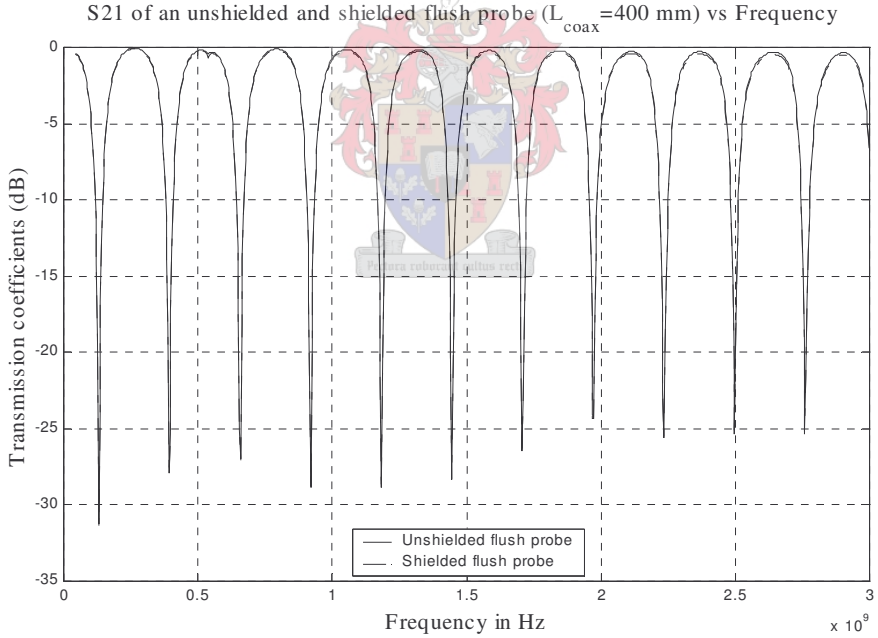

Fig. 2.12 S_{21} (dB) measurement results of the unshielded and shielded flush monopole

Figures 2.13 to 2.17 show a comparison of measured and simulated data of reactance graphs of bare monopoles (i.e. monopoles of sizes: 40 mm, 20 mm, 10 mm, 2.5 mm and flush) plotted against h/λ. Measurement results were obtained using the T-resonator measurement technique and numerical predictions were obtained using

FEKO. Figures 2.16 to 2.17 show measured results of a flush monopole reactance against frequency using the T-resonator technique.

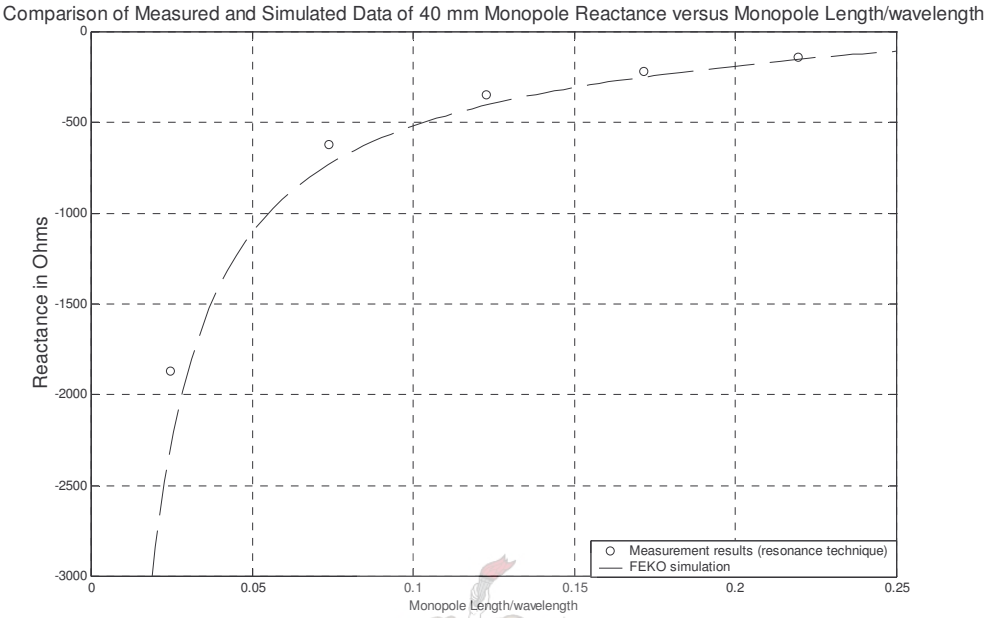

Fig. 2.13 Comparison of measured and simulated reactance graphs of a 40 mm monopole (FEKO numerical predictions done by Marc Rütshln)

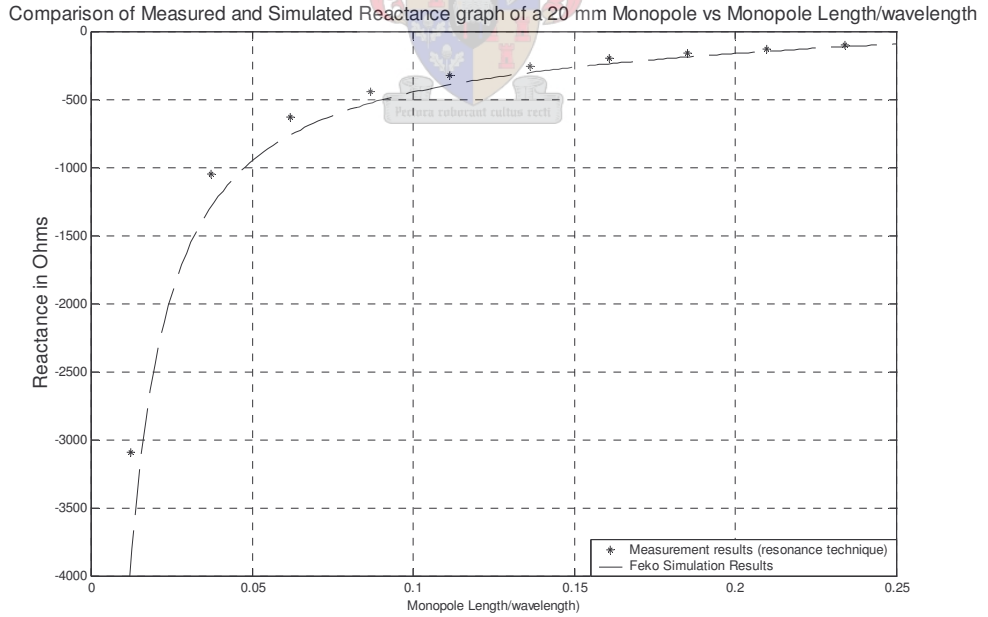

Fig. 2.14 Comparison of measured and simulated reactance graphs of a 20 mm monopole

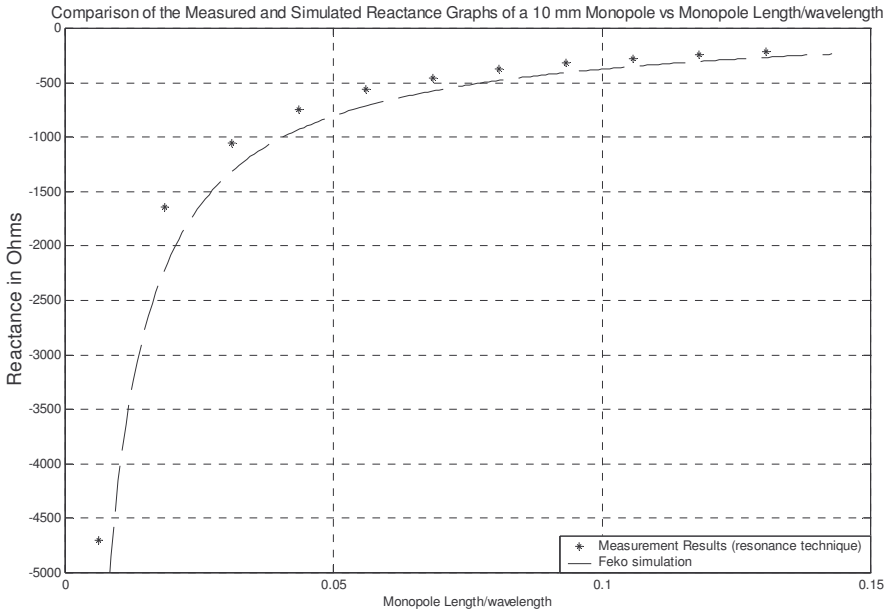

Fig. 2.15 Comparison of measured and simulated reactance graphs of a 10 mm monopole

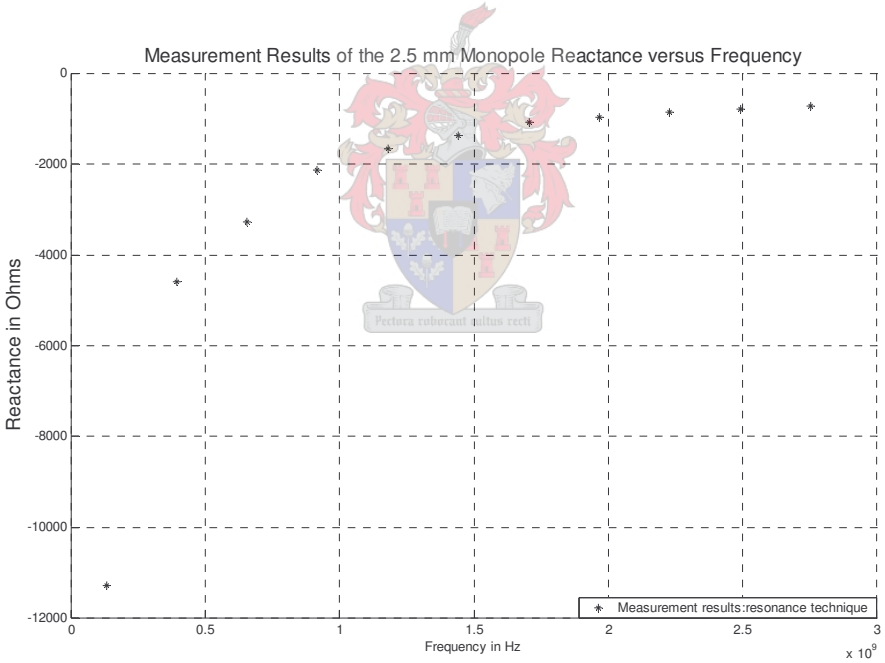

Fig. 2.16 Measured reactance graphs of a 2.5 mm monopole

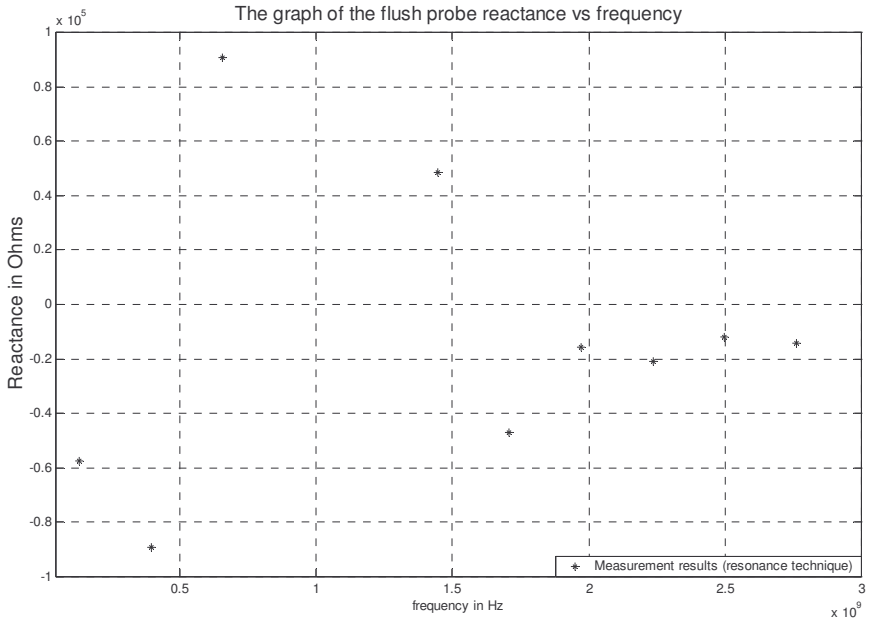

Fig. 2.17 Measured reactance graphs of the flush monopole reactance

Figures 2.18 to 2.20 show a comparison of measured and simulated graphs of capacitance for bare and insulated monopoles plotted against frequency. Measurement results were obtained using the T-resonator technique and numerical predictions were obtained using FEKO.

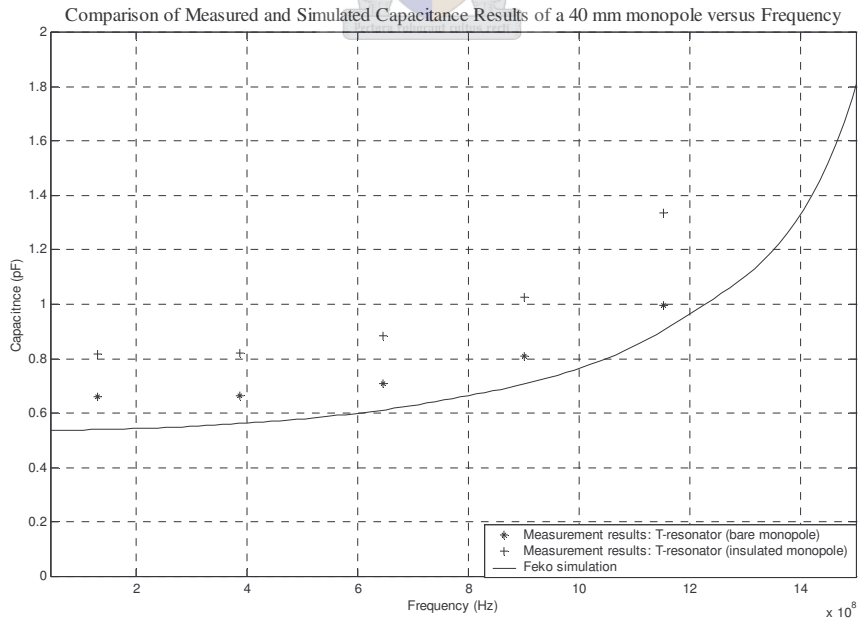

Fig. 2.18 Comparison of the measured and simulated capacitance graphs of the 40 mm monopole versus Frequency

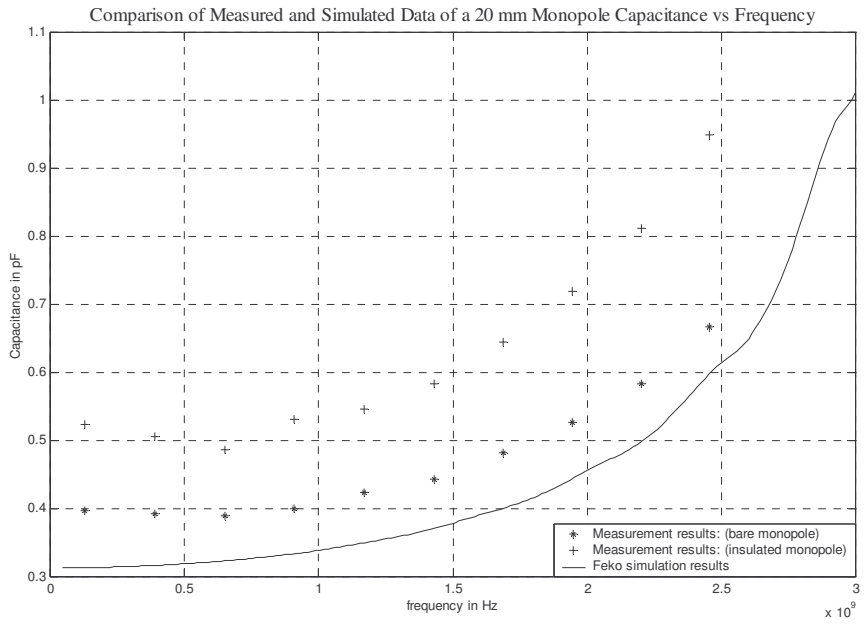

Fig. 2.19 Comparison of the measured and simulated capacitance graphs of the 20 mm monopole versus Frequency

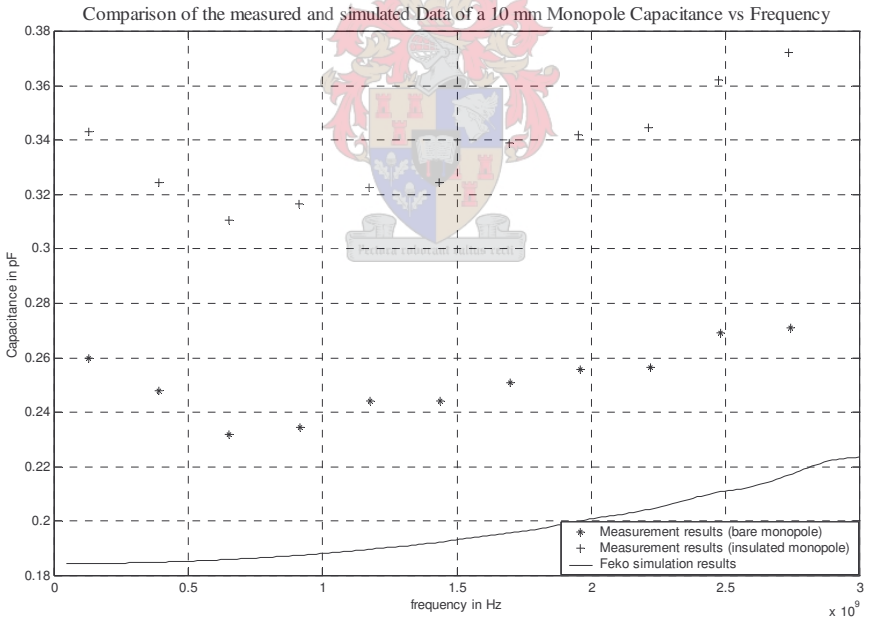

Fig. 2.20 Comparison of the measured and simulated capacitance graphs of the 10 mm monopole versus Frequency

Table 2.1 below tabulates a comparison of this work's results for the monopole capacitance with the corresponding published data.

Table 2.1: Comparison of the capacitance values for this work with the corresponding published data.

Length of the monopole (mm) (0.141 inch)	Bare (left) and insulated (right) monopole capacitance values (pF): T-resonator technique		Bare (left) and insulated (right) monopole capacitance (pF) [Appendix A]		Experimental (pF) [8]	Numerical [7]	% Agreement
40 mm	0.6606	0.8175	0.718	0.92			
20 mm	0.3970	0.5237	0.32	0.43			
10 mm	0.26	0.343	0.15	0.22			
Flush	0.0211	-	-	-	0.0224	0.0217	5.8 [8] and 2.76 [7]

Fig. 2.21 below illustrates a variation of measured bare and insulated monopole capacitances with length (only the first resonance points for each corresponding monopole were considered).

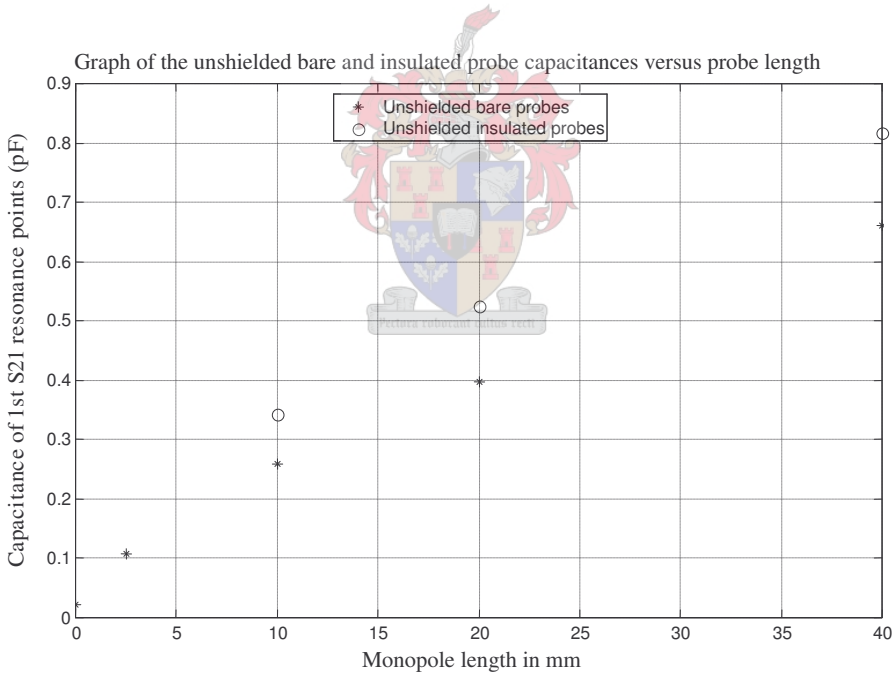

Fig. 2.21 Graphical representation of unshielded bare and insulated monopole capacitances versus monopole lengths

Finally, Fig. 2.22 below illustrates a comparison of measured results of this work with other previous researchers. The measurement results are then compared with simulated data.

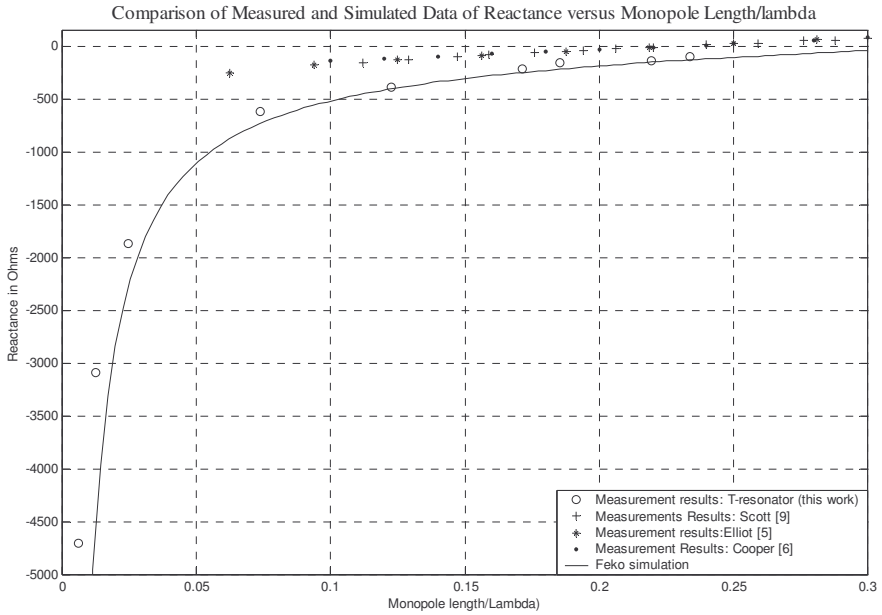

Fig. 2.22 A graphical representation of measured data for reactance determined by the T-resonator technique of this thesis along with other published results

2.4 Discussions and Conclusion

Great care was taken in obtaining measurements as can be seen in Section 2.2.1. Figures 2.5 to 2.12 illustrate transmission coefficient graphs of various monopoles at resonant points with the extracted numerical data presented in Appendix C. To enhance accuracy, the resolution around each resonant point was improved to establish the exact tuning point. It can be seen that the resonant points of transmission coefficient graphs at frequencies closer to the resonant frequency of each monopole are not accurately determined because the quasi-static lumped element circuit model of the monopole admittance breaks down. This limits the resonant method to frequencies below the resonant frequency of each monopole.

Reactance graphs for this work are found in Figures 2.13 to 2.17. It can be seen that the T-resonator technique compares well with simulated data. Graphical representation of capacitance for first transmission resonant points of each monopole is shown in Fig. 2.21. The capacitance values increase linearly with length as expected for electrically short monopoles. Also, it can be observed that insulated

monopoles have slightly greater capacitance than bare probes. This is expected because of the polarization density induced in the dielectric teflon insulating material. Capacitance graphs of various monopoles are also shown in Figures 2.18 to 2.20.

Table 2.1 tabulates a comparison of measurement results of this work with the previous researchers. The measured capacitance for a flush probe agrees with that of Kraszewski and Stuchly [8] by 5.8% and by 2.76% with the simulated data by Gajda and Stuchly [7]. Fig. 2.22 illustrates a comparison of this work with other researchers. It can be seen that the T-resonator technique compares well with simulated data.

It can be concluded that the T-resonator method by Kraszewski and Stuchly [8] has been extended to measure capacitance of monopoles of various sizes including the flush probe. The accuracy of this technique is affected by the shift in resonant frequencies of open- and short-circuited monopoles due to junction effects. Eq. 2.22 is derived to cater for the possible junction effects. The T-resonator technique can yield good measurement results and compares well with simulated data and previous research work. It has also been established that the applications of the T-resonator technique is restricted to frequencies below the first resonance of monopoles, i.e. to frequencies where the monopole is electrically short. The capacitance for a flush probe agrees with the published data by less than 10%, which indicates that the technique is also good for flush-mounted electrically short monopoles.

Chapter 3

Measurement of the Radiation Resistance of Electrically Short Monopoles at Radio Frequencies Using a T-resonator Technique

This Chapter presents a development of a T-resonator technique to determine radiation resistance of electrically short monopoles. A rigorous analytical model to accurately measure radiation resistance of electrically short monopoles applicable for both flush and extended centre conductor cases at Radio Frequencies is presented. Measurements were taken using an HP 8510C network analyser in the frequency range 45 MHz to 3 GHz. Measurements for the unshielded monopoles were performed in the anechoic chamber to minimize obstacle and room reflections. By comparing the depth of the transmission coefficient null points of shielded and unshielded monopoles at various resonant frequencies and analysing, the resistance of the monopoles can be determined. The method is applicable for both flush and the extended centre conductor cases. The experimental results are compared with FEKO numerical predictions and with previous work research in this field. Both bare and insulated monopoles were studied.

3.1 Derivation of the Equation to Compute Coaxial Monopole's Radiation Resistance

Consider the equivalent circuit of the coaxial line model shown below that shunts the microstrip line in the case when the coaxial line is at resonance (see Fig. 1.2 for a full view of the coupling device).

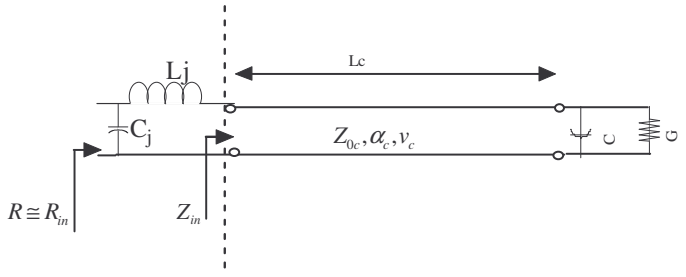

Fig. 3.1 Open-circuited coaxial line model that shunts the microstrip line (L_j and C_j represent junction effects).

From Fig. 3.1 above, the input impedance $Z_{in} = R_{in}$ at resonance. Also, the total resistance including junction effects, $R_{tot} \cong R_{in} = R$ since the junction equivalent transmission line model is electro-magnetically too short (less than 1mm) as compared to the coaxial line to significantly transform R_{in}. From the transmission line theory [15, Section 5.11], R_{in} is given by:

$$R_{in} = Z_{0c}\left(\frac{1+\rho_{in}}{1-\rho_{in}}\right) = Z_{0c}\left(\frac{1+e^{-(2\alpha_G+2\alpha_c L_c)}}{1-e^{-(2\alpha_G+2\alpha_c L_c)}}\right) \qquad (3.1)$$

Considering Equations 2.1 and 2.2 in Chapter 2 and noting that $\alpha_G = G\,Z_{0C} << 1$ and that $-\phi_{in} = n\pi$ for all n odd, then the input reflection coefficient is given by

$$\rho_{in} = -\exp\{-2(\alpha_G+2\alpha_c L_c\} \quad \text{for all n odd} \qquad (3.2)$$

At resonance, it can be shown that the equivalent resistance as shown if Fig. 3.1 is finally given by:

$R_{in} = R \cong (GZ_{0c} + \alpha_c L_c)Z_{0c}$ for all n odd at quarter wave resonance points. (3.3)

Assuming that the characteristic impedances of both the coaxial line and microstrip line are equal ($Z_{0c} = Z_{0m} = Z_0$) and that the microstrip line is perfectly matched to the load at port 2 of the HP 8510C network analyser, the coax-microstrip equivalent circuit at odd quarter wave length resonances will then be as shown in Fig. 3.2 below:

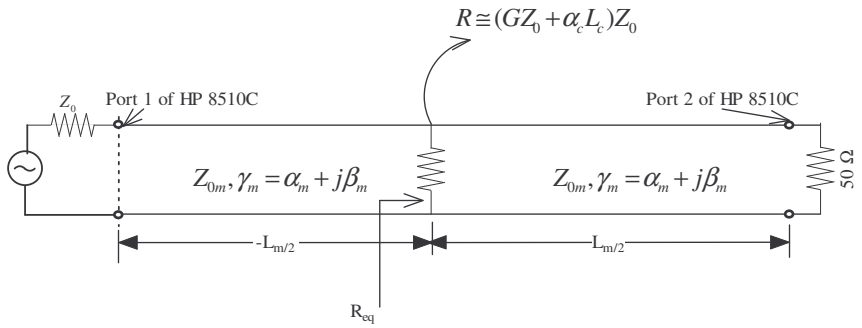

Fig. 3.2 Equivalent circuit of the coupling system at odd quarter wave length resonance

From Kirchhoff's voltage law, the R_{eq} from two parallel impedances is given by:

$$R_{eq} = RZ_0/(R + Z_0) \tag{3.3}$$

For the electric field continuity at the junction point, it is required that the incident voltage (V_{inc}) and reflected (V_{refl}) voltage must be equal to the transmitted voltage (V_{trans}). That is,

$$V_{inc} + V_{refl} = V_{trans} \quad \text{or} \quad \frac{V_{trans}}{V_{inc}} = 1 + \rho \tag{3.4}$$

The reflection coefficient in Eq. 3.4 can be obtained from Eq. 3.3 as follows:

$$\rho = \frac{R_{eq} - Z_0}{R_{eq} + Z_0} = \frac{-Z_0}{2R + Z_0} \tag{3.5}$$

The incident (V_1) and transmitted (V_2) voltages at ports 1 and 2 (see Fig. 3.2) are given by

$$V_{1(z=-L_m/2)} = V_{inc} e^{\alpha_m L_m/2} e^{j\beta L_m/2} \tag{3.6}$$

$$V_{2(z=L_m/2)} = V_{trans} e^{-\alpha_m L_m/2} e^{-j\beta L_m/2} \tag{3.7}$$

$$\therefore \; S_{21} = \left(\frac{V_{trans}}{V_{inc}}\right) e^{-\alpha_m L_m} e^{-j\beta L_m} \tag{3.8}$$

On substituting Equations 3.4 and 3.5 in 3.8 and rearranging, it can be shown that the magnitude of the transmission coefficient at odd quarter-wave resonance points is given by:

$$\left|S_{21}\right| = \left(\frac{2(R/Z_0)}{1+2(R/Z_0)}\right) e^{-\alpha_m L_m} \tag{3.9}$$

which reduces to:

$$|S_{21}| = (2R/Z_0)e^{-\alpha_m L_m} \quad \text{if } R << Z_0 \tag{3.10}$$

On substituting $R \cong (GZ_0 + \alpha_c L_c)Z_0$ into Eq. 3.10 we get:

$$|S_{21}| \cong 2(GZ_0 + \alpha_c L_c)e^{-\alpha_m L_m} \tag{3.11}$$

The magnitude of the transmission coefficient in E.q. 3.11 can also be expressed in Decibels as follows:

$$|S_{21}|_{dB} \cong 20\log_{10}(|S_{21}|) = 6 - 8.686\alpha_m L_m + 20\log_{10}(GZ_0 + \alpha_c L_c) \tag{3.12}$$

provided $(GZ_0 + \alpha_c L_c) << 1$

If G = 0, then Eq. 3.11 reduces to

$$|S_{21}|_{Shielded} \cong 2(\alpha_c L_c)e^{-\alpha_m L_m} \tag{3.13}$$

When the monopole is not shielded (G > 0), we have

$$|S_{21}|_{Radiation} \cong 2GZ_0 e^{-\alpha_m L_m} + 2\alpha_c L_c e^{-\alpha_m L_m} = 2GZ_0 e^{-\alpha_m L_m} + |S_{21}|_{Shielded} \tag{3.14}$$

$$\therefore \Delta S_{21} = |S_{21}|_{radiation} - |S_{21}|_{shield} = 2G_{rad} Z_0 e^{\alpha_m L_m} \tag{3.15}$$

The final equation for the radiation conductance is therefore given by

$$G_{rad} = G = e^{\alpha_m L_m}\left(\frac{\Delta S_{21}}{2Z_0}\right) \tag{3.16}$$

where $\Delta S_{21} = |S_{21}|_{\text{radiation}} - |S_{21}|_{\text{shield}}$ is the difference between the measured magnitude of S_{21} null levels for the shielded and unshielded cases. Let us examine the

applicability of the derived equation of radiation conductance using the parameters of the coupling device in Fig. 1.2 by Example 3.1 below:

Example: 3.1

Parameters: L_c (electromagnetic length of the coaxial line) = 0.351m, L_m = 0.3m, α_c = 0.022 Np/m and α_m = 0.024 Np/m. Assume that $Z_0 = Z_{0c} = Z_{0m} = 50\Omega$. On substituting the above parameters in Eq.12 we get

$$\left|S_{21}\right|_{dB} \cong 20\log_{10}(\left|S_{21}\right|) = 6 - 8.686(0.0072) + 20\log_{10}(G(50) + 0.007722)$$

Case 1: When G = 0 (i.e. shielded monopole), Eq. 3.17 becomes

$\left|S_{21}\right|_{dB} \cong= 6 - 0.067 - 42.245 \cong -36dB$, which is accurately measurable with the HP8510C.

Case 2: When G > 0 (i.e. radiating monopole)

Assume that ($GZ_0 \cong \alpha_c L_c$), $\therefore$ 20log10 ($GZ_0 + \alpha_c L_c$) $\cong$ 20log10 (2 X $\alpha_c L_c$) = 6dB + 20log10 ($\alpha_c L_c$). This implies that the transmission coefficient null will decrease by approximately 6 dB. This also can be accurately measurable using the HP 8510C network analyser.

Therefore, the radiation conductance can be obtained experimentally by making accurate $\left|S_{21}\right|$ measurements at odd quarter-wave resonance points when:

(i) the probe is shielded using the Wheeler [16] cylindrical shield and

(ii) the probe is radiating over ground plane.

The difference in the two cases can then be used to compute the radiation conductance. The experimental setup is the same as the one described in Section 2.2.1 of Chapter 2.

3.2 Results

Resonance graphs of unshielded and shielded monopole measurement results are the same as those presented in Chapter 2 (Figures 2.5 to 2.12). A graphical representation of measured monopole's resistance at various resonance frequencies and FEKO simulated data of resistance for bare monopoles is shown in Figures. 3.3 to 3.5 below. Only bare monopoles ranging from sizes 10 mm to 40 mm were simulated with FEKO. The numerical results of various sizes of monopoles including those of 2.5 mm and flush are tabulated in Appendix C.

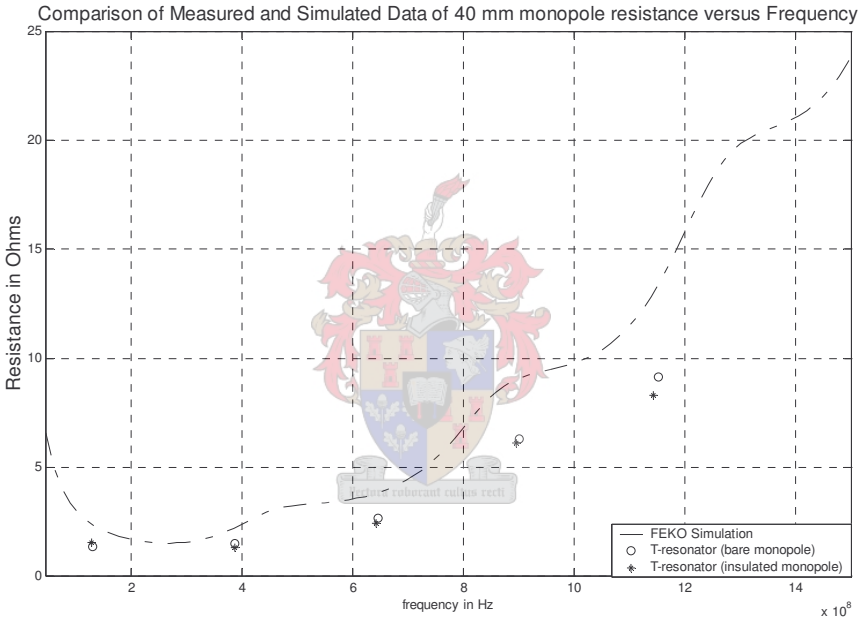

Fig.3.3 Comparison between measured and simulated results of the 40 mm monopole resistance

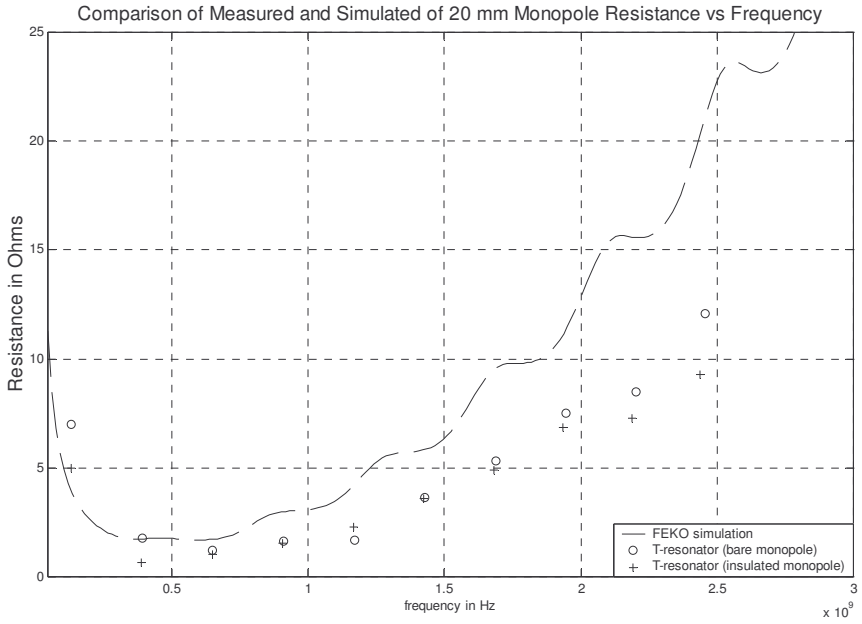

Fig.3.4 Comparison between measured and simulated results of the 20 mm monopole resistance

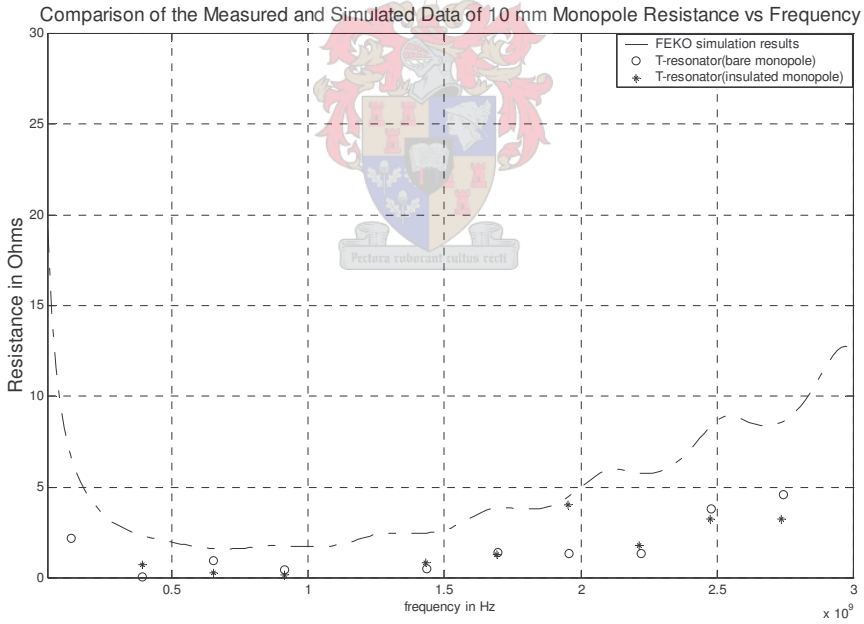

Fig.3.5 Comparison between measured and simulated results of the 10 mm monopole resistance

Figures 3.6 to 3.8 show a graphical representation of measured monopole's resistance at various resonance frequencies and FEKO simulated data of resistance for bare monopoles plotted against monopole length over wavelength (h/λ). Only monopoles of sizes 10 mm to 40 mm are shown.

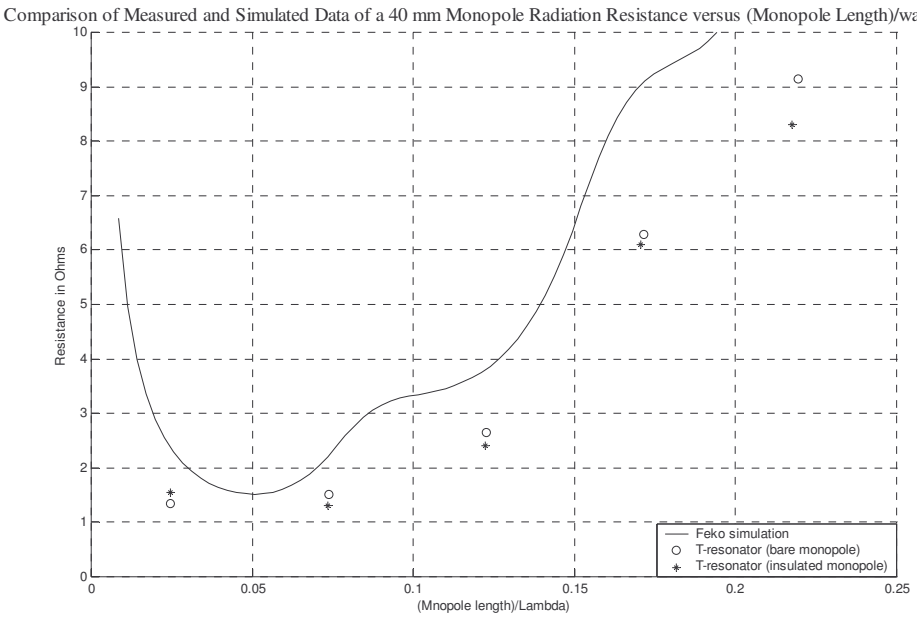

Fig.3.6 Comparison between measured and simulated results of the 40 mm monopole resistance

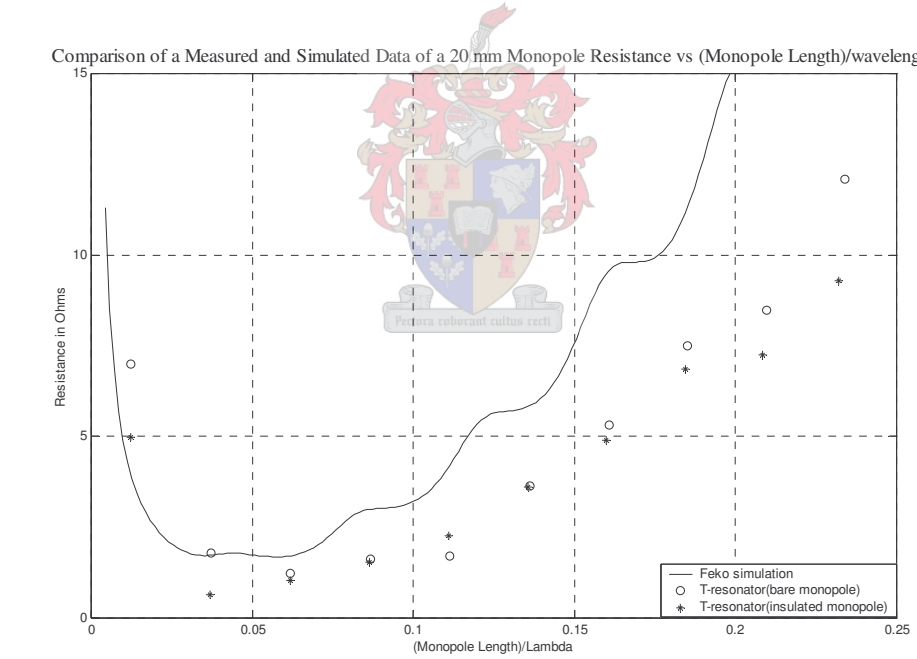

Fig.3.7 Comparison between measured and simulated results of the 20 mm monopole resistance

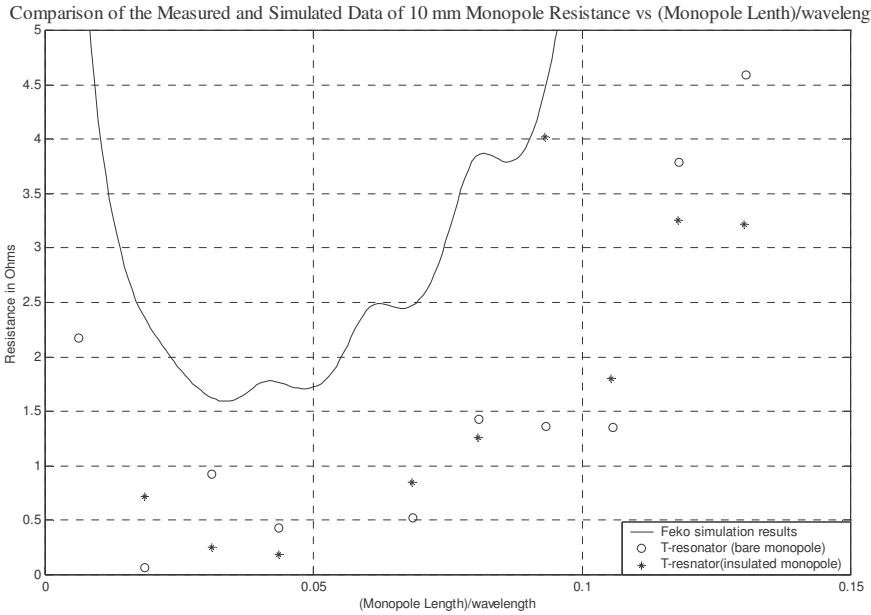

Fig.3.8 Comparison between measured and simulated results of the 10 mm monopole resistance

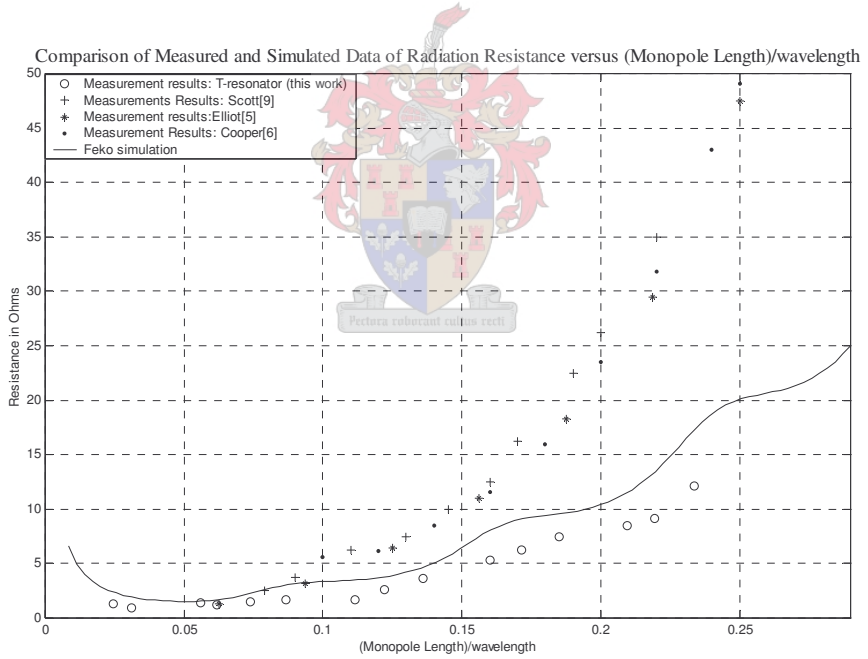

Fig.3.9 A graphical representation of measured data for the radiation resistance determined by the T-resonator technique of this thesis along with other published results

3.3 Conclusion

Detailed measurement results for this work are tabulated in Appendix C. The technique is good for $0.0062 < h/\lambda < 0.2338$. It can be observed in Fig. 3.9 that the technique measures at even lower monopole length/wavelength (h/λ) than other researchers. It also compares well with the simulation data and previous research work. The technique is applicable for frequencies lower than the resonance frequency of the monopole and fails at frequencies near or beyond the resonant frequency of the monopole where the electro quasi-static lumped circuit model of the monopole admittance is invalid. Both bare and insulated monopoles were investigated. It can be concluded that an alternative technique capable of yielding good results is developed and is useful in the indicated ranges.

Chapter 4

Conclusion

The determination of monopole impedance parameters is based on the idea provided by Kraszewski and Stuchly [8]. In this work, their model was further developed to measure capacitance and radiation resistance of extended centre conductor cases. A carefully designed one port coaxial-microstrip coupling system was designed to take measurements using HP 8510C Network Analyser.

Rigorous analytical derivation and experimentally verification of equations to compute the capacitance of monopoles confirms that the accuracy of this model is affected by the shift in measured resonant frequencies due to junction effects. These effects have been catered for in the equation used to analyze experimental results (see Eq. 2.22, Chapter 2). Also, the derived equation is designed to measure frequency of the monopole using network analyzer, which is capable of measuring frequency with high precision. The technique is capable of accurately yielding sub-pico Farad capacitances in the range 0.0211 pF to 1 pF at $0.0062 < h/\lambda < 0.2338$ and compares very well with simulation data than other researchers as can be seen in Chapter 2 experimental results. The capacitance for a flush-mounted coaxial line compares very with the ones obtained by Kraszewski and Stuchly [8] by 5.8% and by 2.76% with the simulated data (FEM and MoM) by Gajda and Stuchly [7]. This shows that the developed technique is comparable with other independent research work.

This work further presents a rigorous development of analytical method suitable to determine the challenging radiation resistance of electrically short monopoles at Radio Frequencies. The technique is capable of yielding radiation resistance in the range 0.9245 to 12 Ohms at $0.0062 < h/\lambda < 0.2338$ and compares relatively well with simulation data than other researchers as shown in Chapter 3.

It can be concluded that a T-resonator experimental technique suitable for measuring capacitance and radiation resistance, both flush and extended centre conductor cases, of electrically short monopoles at Radio Frequencies has been developed.

Future research work will focus on the experimental verification of the coaxial probe coupling model by predicting and measuring the signal delivered to a spectrum analyser when the monopole is in a known electromagnetic field.

Bibliography

[1] H. Levine and C.H. Papas, "Theory of the circular diffraction antenna", *Journal of applied physics*, vol. 22, no.1, January 1951, pp. 29-42.

[2] N. Marcuvitz, *Waveguide handbook*, Peter Peregrinus, London, UK, 1951, pp. 213-216.

[3] J. Galejs, *Antennas in inhomogeneous media*, Pergamon Press, Oxoford, 1969, pp 39-44.

[4] R.W.P. King, *Tables of antenna characteristics,* IFP/Plenum, New York, 1971, pp 29-32.

[5] R.S. Elliott, *Antenna theory and design, Prentice* Hall Inc., New Jersey, 1981, pp352-354.

[6] L.J. Cooper, "Monopole antennas on electrically thick conductors", Ph.D. dissertation, Harvard Univ., Cambridge, MA, Mar 1975.

[7] G.B. Gadja and S.S. Stuchly, "Numerical analysis of open-ended coaxial lines", *IEEE Transactions on Microwave Theory and Techniques*, vol. MTT-31, no.5, May 1983, pp. 380-384.

[8] A. Kraszewski and S.S. Stuchly, "Capacitance of open-ended dielectric-filled coaxial lines-experimental results", *IEEE Transactions on Instrumentation and Measurement,* vol. IM-32, no.4, December 1983, pp-517-519.

[9] W.R. Scott JR. and G.S. Smith, "Dielectric spectroscopy using monopole antennas of general electrical length", *IEEE Transactions on Antennas and Propagation*, vol. AP-34, no.7, July 1986, pp-919-929.

[10] D.K. Misra, "A quasi-static analysis of open-ended coaxial lines", *IEEE Transactions on Microwave Theory and Techniques*, vol. MTT-35, no.10, August 1987, pp. 925-928.

[11] J.G. Maloney, G.S. Smith, and W.R. Scott, JR, "Accurate computation of the radiation from simple antennas using the Finite-Difference Time-Domain method", *IEEE Transactions on Antennas and Propagation*, vol.38, no. 7, July 1990, pp. 1059-1068.

[12] G.S. Smith, *An introduction to classical electromagnetic radiation*, Cambridge University Press, United Kingdom, 1997, pp 599-604.

[13] FEKO User's Manual, Suite 4.0, EM Software & Systems-S.A., Stellenbosch, South Africa, Dec. 2002.

[14] R.L. Peterson and R.F. Dryton, "A CPW T-resonator technique for electrical characterization of microwave substrates", *IEEE Microwave and Wireless Components Letters*, vol.12, no.3, March 2002, pp.90-92.

[15] S. Ramo, J.R. Whinnery, and T. van Duzer, *Fields and waves in communication electronics*, John Wiley and Sons, Inc., New York, 1994, Sec. 5.7, 5.11 8.10, 10.5, 11.7 and 12.3.

[16] H.A. Wheeler, "The radian sphere around a small antenna", *Proc. I.R.E.*, August 1959, pp. 1325 – 1331.

Appendix A

IEEE Africon 2002

REACTANCE OF ELECTRICALLY SHORT RADIO FREQUENCY COAXIAL PROBES

PM Kwinana and JH Cloete
Dept. of Electrical and Electronic Engineering, University of Stellenbosch, Stellenbosch, South Africa

ABSTRACT

An experimental technique is presented to determine the aperture reactance of a short, radio frequency (RF) coaxial probe. The method is based on the inversion of the measured reflection coefficient at the probe's input port. The work was done at 500 MHz using an HP8510C network analyzer and high quality calibration standards. For precise inversion the attenuation and phase constants of the coaxial line must be determined with high accuracy. To a good approximation the measured probe capacitance was found to increase linearly with length from the value for a flush probe. This allows the CW capacitance of a short probe, with length up to 1/10 free-space wavelength, to be modeled using a simple two-term model. Bare and insulated probes, both shielded and unshielded, were studied.

1. INTRODUCTION

Coaxial probes are used in various fields such as permittivity measurements, biomedical techniques, and in near-field metrology [1]-[7]. The aperture admittance of the coaxial line is needed in the Thévenin equivalent circuit of the coaxial probe, both in its role as receiver and as source [8]-[9]. The development of miniature electric field probes, suitable for quantitative sensing of the field at a point in a measurement space, has been advancing for decades [1]-[4], [6] – [7].

Burkhart suggests that an open-ended semi-rigid coaxial probe, inserted no more than flush, with a ground plane is the "convenient and accurate" way to measure electric fields. He argues that this configuration provides high spatial resolution of the field because its diameter is a small fraction of a wavelength for the frequencies of interest [6]. It also allows the coupling to be analyzed quasi-statically. We note, however, that flush mounted probes have obvious practical limitations, for example when the volumetric field in the vicinity of a complex radiator is required.

The input impedance and voltage source models developed by King *et al.* are suitable for electrically short probes with protruding center conductor [10]. However, the model fails for flush center conductors, as in Burkhart's case, or in the case where the center conductor recedes beyond the aperture.

We seek a probe model that is applicable for the recessive, the flush, and the extended center conductor cases. As a first step we present an experimental method based on reflection coefficient measurements to accurately obtain the aperture reactance of an electrically short, open-ended, coaxial line. The center conductor may be flush or extend beyond the aperture plane.

The coaxial line properties were first obtained from the measured reflection coefficient. The line was terminated in a short circuit. Then the measured input reflection coefficient data were inverted to obtain the aperture reactance of an open-ended coaxial line. All measurements were performed on an HP8510C network analyzer.

2. DETERMINATION OF THE COAXIAL LINE PROPERTIES

Consider a low-loss semi-rigid (UT141A-SP) [11] coaxial line as illustrated in Fig.1. The coaxial line is dielectric-filled with PTFE [12]. The diameters of the center conductor and PTFE, are 2a=0.91 mm and 2b=2.98 mm. The diameter of the copper screen is 3.58 mm [11].

Relevant coaxial line properties such as the attenuation constant, phase velocity, and relative permittivity were obtained using transmission line theory [13] and experimental techniques as explained below.

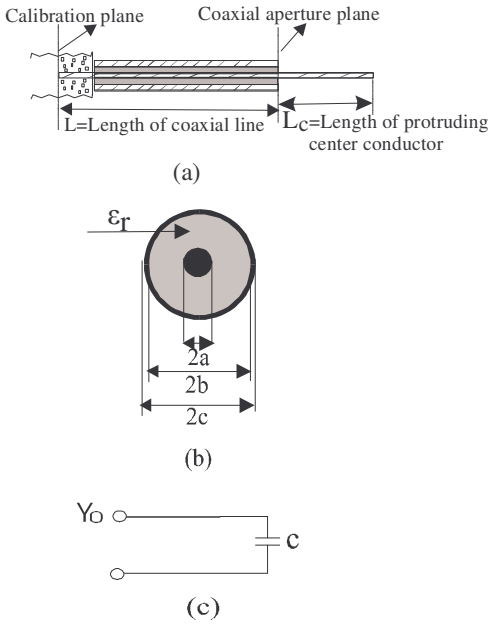

Figure 1: (a) Axial cross-section of an unshielded open-ended coaxial line: (b) Transverse cross-section of an unshielded open-ended coaxial line (c) Equivalent circuit

Appendix A

of a shielded coaxial tip (i.e. on suppression of probe radiation by a conducting cylinder)

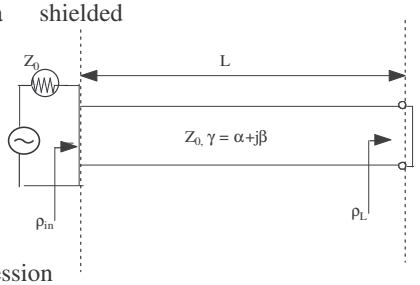

(a)

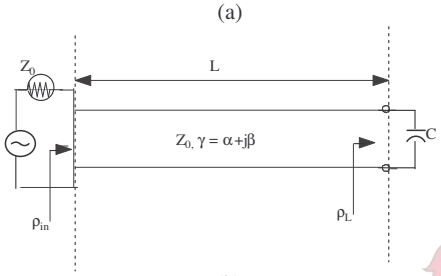

(b)

Figure 2 (a): Short-circuited coaxial line model. (b) Open-circuited coaxial line model

2.1 Attenuation constant of the coaxial line

A coaxial line (UT-141A-SP) of length 400±0.01 mm was used. A brass-shorting cap was carefully soldered on one end of the coaxial line. The length of the coaxial line was measured using a digital venier caliper. A Suhner SMA female connector was used at the other end. The standards definitions of an HP85052D 3.5 mm economy calibration kit (serial no. 3101A03709) were loaded into HP8510C memory. Female standards were used. The reflection coefficient measurements were obtained at 500 MHz with reference to the calibration plane shown in Fig.1. Results are given in Table 1.

Consider the transmission line model representing the coaxial line in Fig.2(a), with [13]

$$\rho_{in} = \rho_L e^{-2\gamma L} \quad (1)$$

where ρ_{in} is the input reflection coefficient at the measurement plane and ρ_L is the reflection coefficient at the load. The propagation constant of the line is $\gamma = \alpha + j\beta$, with α and β the attenuation and phase constants. L is the length of the coaxial line, measured from the calibration plane to the tip of the coaxial line aperture plane as shown in Fig.1. The brass-shorting cap is assumed to be "perfect", thus

$$\rho_L \approx -1. \quad (2)$$

The input reflection coefficient is then

$$\rho_{in} = -e^{-2\alpha L} e^{-j2\beta L}. \quad (3)$$

with magnitude

$$|\rho_{in}| = e^{-2\alpha L}. \quad (4)$$

The value of attenuation constant at 500 MHz was obtained from the measured input reflection coefficient magnitude, and the length of the short-circuited coaxial probe. Table 1 gives the measured result. The attenuation is 0.27 dB/m, which agrees with the manufacturer's value within 17.4%.

2.2. Phase velocity of the coaxial line

The phase constant was first estimated using

$$\beta_{estimate} = 2\pi f/v, \quad (5)$$

with phase velocity $v=c/\sqrt{\varepsilon_r}$, f = 500 MHz, and with $\varepsilon_r \approx 2.03$ estimated for the dielectric from

$$\varepsilon_r = ((60/Z_0)\ln(b/a))^2 \quad (6)$$

for the Z_O=50 Ω coaxial line. The short-circuited coaxial line of Section 2.1 was used to obtain phase measurements using the network analyzer HP8510C at 500 MHz. From Equation 3, it can be shown that the corresponding angles of the terms are related as follows:

$$\angle\rho_{in} = \angle\rho_L - 2\beta L \quad (7)$$

where $\angle\rho_L = \pi$ for a short-circuited line. The angle, as measured by the network analyzer, is related to $\angle\rho_{in}$ by

$$\phi_m = \angle\rho_{in} + 2\pi n \quad (8)$$

where n is an integer and $-\pi < \phi_m \le \pi$ is the principal value of the phase angle. On combining and rearranging Equation 7 and 8, it can be shown that the expression for the phase velocity is

$$v = 2fL/((n+1/2) - (\phi_m/2\pi)) \quad (9)$$

The first estimate of the phase velocity was used in Equation 9 to obtain the value n=1. With n known, an improved estimate of v is obtained also from Equation 9. The resulting normalized phase velocity is 0.700. The phase constant is hence 14.96 rad/m. It agrees with the

Appendix A

first estimate to within 0.2%. The relative permittivity is computed to be 2.04. The computed relative permittivity, unlike the value of 2.1 given by Von Hippel [12], is consistent with modern values for pure PTFE.

To quantify phase velocity, uncertainty analysis using corresponding known uncertainty values of coaxial line length, phase angle, and the operating frequency was done. The summary of the uncertainty numerical values is given in Table 2. The dominant error in the phase velocity is due to the phase angle uncertainty. This uncertainty is the source of errors in phase constant and relative permittivity. This indicates that the input reflection

Table1: Experimental results for a short-circuited UT-141A-SP semi-rigid coaxial line at 500 MHz

Termination	Length from the connector mating surface to coaxial aperture plane (mm)	Reflection coefficient	Attenuation dB/m	Normalized phase velocity (v/c)
Soldered short 1	400	$0.9752\angle -145.85^{o}$	0.27	0.700

Table2: Summary of uncertainties

Quantity	Uncertainty	Comment
Length (L) = 0.4 m	$\pm$ 1x 10^{-5}m	Digital venier caliper
Measured phase angle (ϕ_m) = -2.546 rad	$\pm$ 1.4x 10^{-2} rad	HP8510C Specification
Measured frequency (f) = 500 MHz	$1{:}10^{9}$	HP8510C synthesized frequency generator
Estimated phase velocity (v/c) = 0.700	Δ(v/c) = 8.3x10^{-4}	Obtained from Equation 9 using measured data

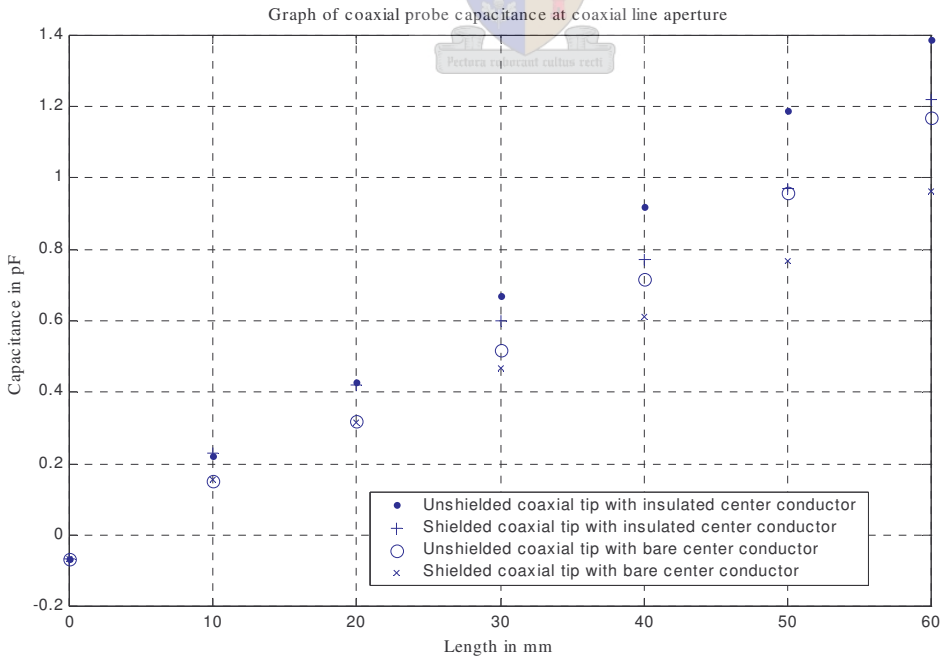

Figure3: Graphs of coaxial line and probe capacitance versus probe length at 500 MHz
(note: 60 mm in air corresponds to $\lambda/10$ at 500 MHz)

Appendix A

coefficient measurements are sensitive to small errors in phase angle.

3. MEASURED REACTANCE OF THE PROBE

The values of attenuation and phase constants of the line are now accurately known. Hence the reflection coefficient measurements at the calibration plane can be transformed to obtain the unknown load reactance at the tip of the coaxial line.

3.1 Energy transfer at the connector interface

The procedure to obtain probe capacitance from the measured input reflection coefficient assumes that the coaxial line and the network analyzer are perfectly matched. In other words, it is assumed that the only source of a reflected wave is the discontinuity offered by the probe. The validity of this assumption was examined by observing the discontinuity presented by the input SMA connector in both the time and frequency domains.

Calibration was carried out as outlined in Section 2. The stepped frequency measurements were taken in the 45 MHz to 20 GHz band. The network analyzer was then used to transform the frequency-domain data to a time-domain impulse response of the system.

The only prominent synthetic pulses that were observed in the time domain were located at the connector interface, its solder joint with the semi-rigid line, and at the end of the line.
For the frequency band mentioned above, the magnitude of the measured reflection coefficient at the connector interface was -43 dB. This corresponds to a deviation in the characteristic impedance magnitude of less than 1.2% from 50 ohms. The rest of the line was essentially perfectly matched. Since we are working with almost total reflection by the probe the effect on accuracy of the connector discontinuity is negligible. Also note that the cut-off frequency for the first higher order mode in the coaxial line is 34.7 GHz, from

$$\pi(a+b)/n \qquad (10)$$

where n =1 for the first order coaxial mode and a and b are radii of the inner conductor and dielectric [13]. This is well above the frequency of operation, i.e. 500 MHz, which means that higher order modes cannot propagate. It is therefore valid to use a TEM transmission line model.

3.2 A Wheeler radiation shield for the coaxial probe

Wheeler's radiation shield [14] can be used to measure antenna efficiency [15]. Here we use the Wheeler shield to reduce the radiation conductance to zero, while causing negligible disturbance to the reactive near field that is dominant in the region

$$r \le 1/k \qquad (11)$$

centered on the probe base, where $k = 2\pi/\lambda$ [13]. The shield dimensions were computed according to Wheeler's theory. The radius and height of the conducting cylinder are 100 mm and 180 mm. The tip of the coaxial line was placed tight and flush at the center of the conducting cylinder's closed bottom to ensure good ohmic contact.

The cut-off frequency for the first order TM mode of the conducting cylinder is 1.15 GHz. Since the operating frequency is less than the cut-off frequency, the radiation will be attenuated [13]. In this case the attenuation is approximately 200 dB/m.

3.3 Coaxial probe capacitance measurements and sensitivity analysis

The input reflection coefficient measurements of the open-ended coaxial were obtained for two different cases at 500 MHz: (i) When a 60 mm copper screen is removed from the tip of the coaxial line and the insulated conductor is cut back in steps of 10 mm up to a flush transition point and (ii) When the screen and dielectric are removed in the same way.

By making use of Equation 1 and known values of attenuation and phase constants, input reflection coefficient measurements were transformed and aperture capacitance were computed for both cases. A graphical representation of results is given in Fig.3.

All the graphs in Fig. 3 converge to one point when the center conductor is shortened to a flush transition point. The coaxial probe at the flush transition point has a capacitance of –0.066 pF. This is obviously a non-physical result. In [4] Kraszewski and Stuchly measured 0.0224±0.00146 pF with 95% confidence for a 0.141-inch semi-rigid line using a resonance technique.

To quantify measured capacitance results, a sensitivity analysis for the flush transition point was performed. This point was chosen since it is the critical point for all the graphs in Fig 3. From Figure 2(b),

$$\rho_L = (Z_L - Z_o)/(Z_L + Z_o) \qquad (12)$$

On dividing by Z_L on the right hand side of Equation 12 and making use of the fact that $1/Z_L = Y_L \cong jwC$ for a short shielded probe where $\omega=2\pi f$ and C the capacitance, ρ_L can be written as

$$\rho_L = (1 - jZ_o\omega C)/(1 + j Z_o\omega C) \qquad (13)$$

Letting $b = Z_o\omega C$, and on estimation of b using the published value of C [4] at 500MHz, it can be shown that $b << 1$. Using this approximation in Equation 13, it can be shown that

Appendix A

$\angle \rho_L \cong -2b.$ (14)

On rearranging Equations 7 and 8 and making use equation 14, the probe capacitance can be written as

$$C = (T/2Z_0)(n - \phi_{in}/2\pi) - L/vZ_o \quad (15)$$

where T is the period, v the phase velocity, n an integer and $-\pi < \phi_{in} \leq \pi$ the measured principal value of the phase angle. The value n = 2 is found using the published value of C [4] in Equation 15. Since ΔT is negligible, the capacitance error equation is given by

$$\Delta C = \partial C/\partial \phi_{in} \Delta \phi_{in} + \partial C/\partial L \Delta L + \partial C/\partial v \Delta v \quad (16)$$

The capacitance was first evaluated to be –0.065 pF using Equation 15. The range of ΔC are ± 0.085 pF using Equation 16, partial derivatives and measurement uncertainty values as summarized in Table 3 below.

Table 3: Summary of partial derivatives and uncertainty values

Quantity	Amount	Quantity	Amount
$\partial C/\partial \phi_{in}$	-3.2×10^{-12}	$\Delta \phi_{in}$	$\pm1.4\times10^{-2}$
$\partial C/\partial L$	-95.2×10^{-12}	ΔL	$\pm1\times10^{-5}$
$\partial C/\partial v$	1.54×10^{-19}	Δv	$\pm2.5\times10^{5}$

The dominant errors are due to the first term and the last terms on the right hand side of Equation 16. The capacitance measurement at flush transition point is therefore given by

$C = -0.065 \pm 0.085$ pF. (17)

From the error in Equation 7, it can be concluded that the accuracy in capacitance measurements is limited by the inability to precisely measure phase angle as has been argued in Section 2.2.

4. DISCUSSION OF RESULTS

Great care was taken in obtaining reflection coefficient measurements. All measurements were taken using a high quality calibration kit with precisely defined standards. Values of capacitance are obtained for two different cases as outlined in Section 3.

The equivalent circuit of the shielded coaxial tip is illustrated in Fig 1(c). The capacitance for an electrically short probe is approximately

$$C_{probe} = C_o + L_c C_1 \quad (18)$$

where C_O is the capacitance when the center conductor is flush with the aperture plane, L_c is the length of the protruding center conductor, and C_1 is the capacitance per unit length. This corresponds to a first order Taylor approximation.

From Table 4 below, the distributed capacitance for PTFE dielectric has the largest value of C_1 in comparison to other cases. All capacitance measurements increase essentially linearly with length, as expected for a short probe. As also expected, the values of the slope coefficients are less than the distributed capacitance of the shielded coaxial line: 0.1 pF/mm for PTFE dielectric and 0.05 pF/mm for air dielectric.

Table 4: Slopes of graphs from Fig. 3

Condition	C_1 (pF/mm)
Unshielded coaxial tip with insulated center conductor	0.025
Shielded coaxial tip with insulated center conductor	0.02
Unshielded coaxial tip with bare center conductor	0.02
Shielded coaxial tip with bare center conductor	0.017
Coaxial line distributed capacitance for PTFE dielectric	0.1
Coaxial line distributed capacitance for air dielectric	0.05

The insulated probe has slightly greater capacitance per meter than the bare probe. This is expected because of the polarization density induced in the dielectric sheath.

The difference between the shielded and unshielded graphs in Fig. 3 is presumably due to the charge redistribution when a radiation shield is placed around the coaxial probe. It may also be that we have failed to properly account to the effect of non-zero radiation conductance in the unshielded probe case.

5. CONCLUSION

A first order model suffices for the capacitance of an electrically short probe at a fixed frequency. The coefficients can be obtained by inversion of accurately measured reflection coefficient data.

A simple, but accurate, method has been devised for measuring the phase and attenuation constants of the coaxial line between the connector and the probe. This is necessary because the parameters extracted from the manufacturer's data are not sufficiently accurate for reflection coefficient inversion purposes.

The error in capacitance at the flush transition point is corrected using sensitivity analysis. The upper limit of the corrected capacitance agrees with the one obtained by Kraszewski and Stuchly within 11%.

Work is now underway to obtain a good theoretical model for the radiation conductance of coaxial probes. The predictions of this model will be verified experimentally.

Appendix A

We will be guided by the extensive literature, for example [4]-[7].

Our eventual aim is to obtain an accurate Thévenin equivalent circuit for a coaxial probe, including the flush aperture case.

6. REFERENCES

[1] M. A. Stuchly, M. M. Brady, S. S. Stuchly, and G. Gajda, "Equivalent circuit of an open-ended coaxial line in a lossy dielectric", *IEEE Transactions on Instrumentation and Measurement*, vol. IM-31, no. 31, June 1982, pp. 116-119.

[2] K.F. Staebel and D.K. Misra, "An experimental technique for *in vivo* permittivity measurement of materials at microwave frequencies*", IEEE Transactions on Microwave Theory and Techniques*, vol. MTT-38, no.1, January 1990, pp.8-14.

[3] G.B. Gadja and S.S. Stuchly, "Numerical analysis of open-ended coaxial lines", *IEEE Transactions on Microwave Theory and Techniques*, vol. MTT-31, no.5, May 1983, pp. 380-384.

[4] A. Kraszewski and S.S. Stuchly, "Capacitance of open-ended dielectric-filled coaxial lines-experimental results", *IEEE Transactions on Instrumentation and Measurement,* vol. IM-32, no.4, December 1983, pp-517-519.

[5] N. Marcuvitz, *Waveguide handbook*, Peter Peregrinus, London, UK, 1951, pp. 213-216.

[6] S. Burkhart, "Coaxial E-field probe for high-power microwave measurement", *IEEE Transactions on Microwave Theory and Techniques*, vol. MTT-33, no.3, March 1985, pp. 262-265.

[7] D.K. Misra, "A quasi-static analysis of open-ended coaxial lines", IEEE Transactions on Microwave Theory and Techniques , vol. MTT-35, no.10, August 1987, pp. 925-928.

[8] M.S. Nieman, "The principle of reciprocity in antenna theory", *Proc. I.R.E.*, vol. 31, December 1943, pp. 666-671.

[9] R.E. Collin, *Antennas and radiowave propagation*, McGraw-Hill Book Company, New York, 1985, pp. 294-300.

[10] R.W.P. King, G.S. Smith, M. Owens and T.T. Wu, *Antennas in matter,* The MIT Press, Cambridge, Massachusetts, 1981. Chap. 3.

[11] Huber and Suhner AG Catalogue*,* Herisau, Switzerland, 1985.

[12] Arthur von Hippel, Editor, *Dielectric materials and applications*, Artech House, Boston, London, 1954, p. 332.

[13] S. Ramo, J.R. Whinnery, and T. van Duzer, *Fields and waves in communication electronics*, John Wiley and Sons, Inc., New York, 1994, Sec. 5.7, 8.10 and 12.3.

[14] H.A. Wheeler, "The radiansphere around a small antenna", *Proc. I.R.E.*, August 1959, pp. 1325 – 1331.

[15] J.H. Cloete and C.F. du Toit, "Ridged cavity backed slot antenna with dielectric loading", *Electronics Letters*, vol. 25, no. 5, 2 March 1989, pp 323 – 325.

Principal Author: Phumezo Mzoxolo Kwinana holds an MSc in physics from the University of Fort Hare where he is a physics lecturer. He is currently doing a full-time PhD in Engineering Science at the University of Stellenbosch. He is financially supported by the NRF.

Coauthor: Johannes Hendrik Cloete is a graduate from the Universities of Stellenbosch (BSc, BEng, PhD) and California, Berkeley (MSEE). Between 1969 and 1983 he did spells in the South African Navy; the National Institute for Defence Research, Pretoria; Scientific-Atlanta Inc, Atlanta, Georgia; and the University of Pretoria. Since 1984 he has been a professor in electrical and electronic engineering at the University of Stellenbosch. He works on electromagnetic wave phenomena in stratified, dispersive matter; properties of matter at radio and microwave frequencies; and antenna design. He collaborates with Professor Iain Mason, Sydney University to introduce long-range borehole-radar technology into the South African mining industry for delineation and imaging of ore bodies and fault structures.

Appendix B

IEEE Africon 2004

A T-RESONATOR TECHNIQUE TO MEASURE ADMITTANCE PARAMETERS OF ELECTRICALLY SHORT MONOPOLES AT RADIO FREQUENCIES

PM Kwinana and JH Cloete
Department of Electrical and Electronic Engineering, University of Stellenbosch, Stellenbosch, South Africa

ABSTRACT

An experimental technique to accurately determine admittance parameters of electrically short monopoles is presented. Measurements were taken using an HP 8510C network analyser in the frequency range 45 MHz to 3 GHz. The experimental results compare well with numerical predictions. Both bare and insulated monopoles were studied.

1. INTRODUCTION

Numerical and experimental results for admittance parameters of electrically short monopoles have been reported in [1]–[5] with the emphasis on probe reactance. This paper presents a T-resonator measurement technique to accurately measure both the reactance and the more experimentally challenging radiation resistance of electrically short monopoles. The method is applicable for both the flush and the extended centre conductor cases.

2. EQUATIONS TO COMPUTE MONOPOLE ADMITTANCE PARAMETERS:

2.1 Equation to compute capacitance of the monopole

From transmission line theory, it can be shown that the input reflection coefficient of the coaxial line is given by

$$\rho_{in}=\exp\left\{-2\left(\alpha_G+\alpha_c\right)-2j\left(\Theta_c+\omega\left(\frac{L_c}{v_c}\right)\right)\right\} \quad (1)$$

where $\rho_L = \exp\{-2\alpha_c - j2\Theta_c\}$, $\alpha_G = G\,Z_{0c} << 1$ and $\Theta_c = \omega C Z_{0c} << 1$ for the radiating open-circuited coaxial probe. G and C are the radiation conductance and capacitance. Z_{0c} is the characteristic impedance of the coaxial line and ω is the angular frequency. Lc and v_c are length and phase velocity of the coaxial line. It can be shown that at quarter-wave lengths, the input phase angle is given by

$$-\Theta_{in} = n\pi = 2\omega_{r,n}\,(CZ_{0c} + (L_c/v_c)) \quad (2)$$

where $\omega_{r,n}$ is the angular frequency for each corresponding odd quarter wave lengths and n, the resonance index, is odd. L_c/v_c is quantified by short-circuiting the coaxial line at its output end and measuring frequencies at even quarter wave lengths. Hence,

$$L_c/v_c = (n+1)/4f_{r,n+1} \quad (3)$$

On combining Eq. 2 and 3 and rearranging, it can be shown that the final equation to compute the capacitance of the monopoles is given by

$$C = \frac{1}{4Z_0}\left(\frac{n}{f_{r,n}} - \frac{n+1}{f_{r,n+1}}\right) \quad (4)$$

Equation 4 was derived assuming that there were no junction effects. An investigation to examine the possible junction effects was carried out by analysing the equivalent circuit of the coaxial line with junction parameters. It was found that the junction effects were negligible.

2.2 Equation to compute the conductance of the monopole

At quarter wavelengths, the input impedance of the coaxial line $Z_{in} \approx R_{in}$ where R_{in} is the input resistance of the coaxial line. From Equation 1 it can be shown that at quarter wavelengths, the input resistance of the coaxial line is given by

$$R_{in} = Z_0\left(\frac{1-\rho_{in}}{1-\rho_{in}}\right) = Z_0\left(\frac{1-e^{-(2\alpha_G+2\alpha_c L_c)}}{1+e^{-(2\alpha_G+2\alpha_c L_c)}}\right) \quad (6)$$

Since the junction equivalent transmission line representation is electromagnetically too short as compared to coaxial line to significantly transform R_{in}, the total equivalent resistance of the coaxial line and the junction is hence given by

$$R_{in} = R \approx (2GZ_{0c} + 2\alpha_c L_c)Z_{0c} \quad (7)$$

It can be shown that the magnitude of the transmission line coefficient at odd quarter wavelengths is given by $|S_{21}| = 2(GZ_{0c} + \alpha_c L_c)e^{-(\alpha_m L_m)}$ if $R << Z_0$ where α_m and L_m are attenuation constant and length of the microstrip line. Z_0 is the characteristic impedance of the coaxial and microstrip lines. By making accurate transmission coefficient measurements at odd quarter wave lengths when:

Appendix B

(i) the monopole is shielded and

(ii) the monopole is radiating over a ground plane

it can be shown that the equation to compute the radiation conductance is given by:

$$G_{rad} = G = e^{-\alpha_m L_m}\left(\frac{\Delta S_{21}}{2Z_0}\right) \quad (8)$$

where $\Delta S_{21} = |S_{21}|_{radiation} - |S_{21}|_{shield}$ is the difference between the measured magnitude of S_{21} null levels for the shielded and unshielded cases.

3. MEASUREMENT TECHNIQUE

Consider the one-port coupling model shown in Fig. 1 below.

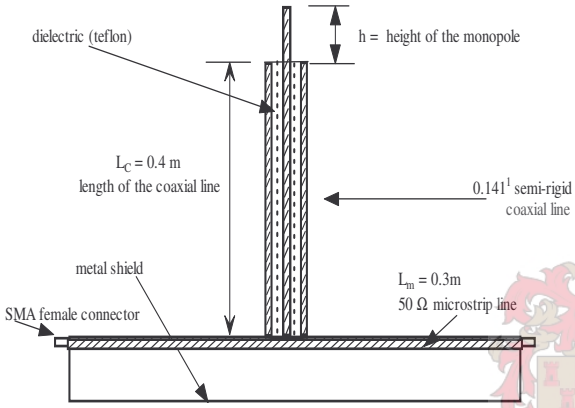

Fig. 1 One port model of the microstrip-coaxial coupling device

The coaxial line that shunts the microstrip line is either open or short-circuited at its output end. When the coupling device is connected to the network analyser, energy is transmitted through from one port to the other and some goes to the coaxial line that shunts the shielded microstrip line. When the coaxial line is either open- or short-circuited at its output end, the line transforms as a series resonant circuit at all odd or even quarter-wave lengths.

By analysing resonant frequencies for both open- and short-circuited coaxial line cases and taking into account junction effects of the coupling model, the capacitance of the monopoles can be obtained. Also, by comparing the depth of the transmission coefficient null points of shielded and unshielded monopoles at various resonant frequencies, the resistance of the monopoles can be determined. Kraszewski and Stuchly have used this method [2] to determine the capacitance of the flush open-ended coaxial lines.

4. EXPERIMENTAL PROCEDURE

All measurements were taken using HP 8510C network analyser in the frequency range from 45 MHz to 3 GHz. Measurements for the unshielded monopoles were performed in the anechoic chamber as shown in Figure 2 below to minimize room and obstacle reflections.

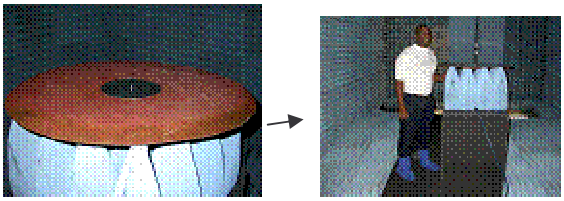

Fig. 2 Procedure for mounting the microstrip-coaxial coupling device in the anechoic chamber

For the first set of measurements, the coupling model was carefully connected to the HP 8510C network analyser that is calibrated using high quality calibration kit with well-defined calibration standards.

The second set of measurements was obtained in the same frequency range as above by directly connecting the coaxial line to one port of the HP 8510C network analyser as shown in Fig 3 below.

Fig. 3 Measurement procedure for the shielded monopoles

The monopoles were cut in steps up to the flush transition point and measurements were taken for each case. Both shielded and unshielded monopoles were investigated.

5. RESULTS

Table 1 tabulates results of this work in comparison with the corresponding published data. The measurements were compared with numerical predictions using the FEKO code [6]. A graphical representation of the measured and simulated results of 40 mm monopole is shown in Figures 2 and 3.

6. CONCLUSION

The resonant method compares well with the simulated data below the resonant frequency of the monopole, but is not applicable near and beyond the resonant frequency of the monopole due to radiation from the currents induced on the cylindrical shield near resonant frequency of the monopole. The measurement results by inversion of measured reflection coefficient method at monopole's input port compares well with the simulated data only at

Appendix B

IEEE Africon 2004

Table 1: Comparison of capacitance results for this work with the corresponding published data

Length of the monopole (mm) (0.141 inch)	Bare (left) and insulated (right) monopole capacitance values (pF): T-resonator technique		Bare (left) and insulated (right) monopole capacitance (pF)[5]		Experimental (pF) [2]	Numerical (pF) [1]	% Agreement Bare (left) and insulated (right)	
40 mm	0.6606	0.8175	0.718	0.92	-	.	8	11
20 mm	0.3970	0.5237	0.32	0.43	-	.	24	21.8
10 mm	0.26	0.343	0.15	0.22	-	.	73	55.9
Flush	0.0211	-	-	-	0.0224	0.0217	6	

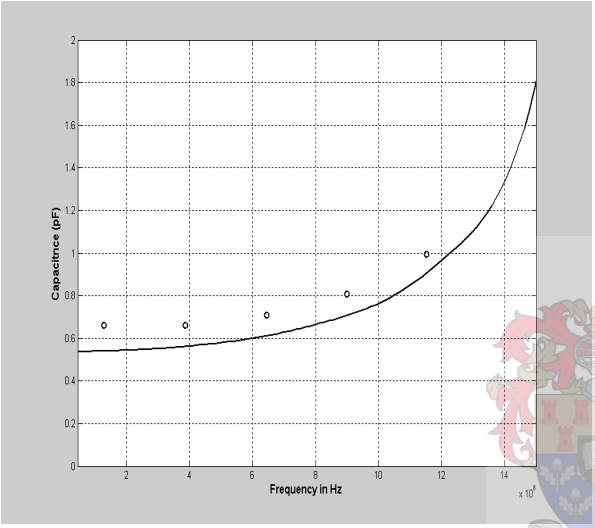

Fig. 4 Comparison of the measured and simulated capacitance results of the 40 mm monopole versus Frequency

O Measured capacitance results (bare monopole: resonance technique)
- Simulated capacitance results (Feko)

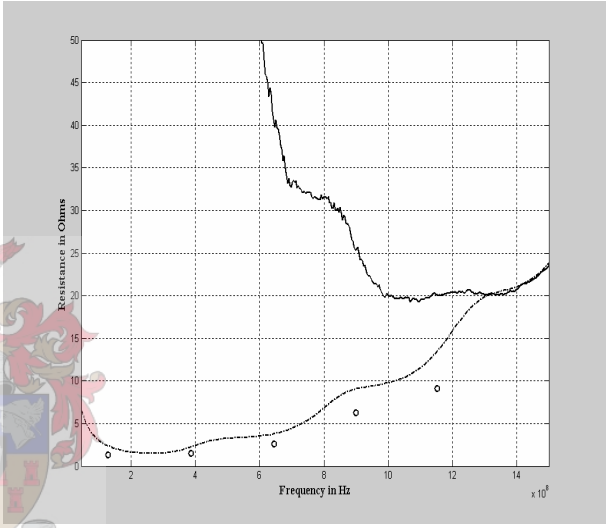

Fig. 5 Comparison of measured and simulated radiation resistance results of the 40 mm monopole versus frequency

O Measured resistance results (bare monopole: resonance technique)
- Measured resistance results (bare monopole: swept frequency)
- - Simulated resistance results (Feko)

high frequencies but fails at lower frequencies. The limiting factor at low frequencies is because the input reflection coefficient measurements are sensitive to small errors in phase angle [5]. It is concluded that the Thévenin equivalent circuit model for lower and higher frequencies can be obtained by using both the resonant and inversion of the measured reflection coefficient at the monopole's input port methods. Future work will focus on the verification of the model by using the monopole to measure the signal delivered to the network analyser when it is immersed in a known electromagnetic environment.

[1] G.B. Gadja and S.S. Stuchly, "Numerical analysis of open-ended coaxial lines", *IEEE Transactions on Microwave Theory and Techniques*, vol MTT-31, no 5, pp 380–384, May 1983.

[2] A. Kraszewski and S.S. Stuchly, "Capacitance of open-ended dielectric-filled coaxial lines–experimental results", *IEEE Transactions on Instrumentation and Measurement,* vol IM-32, no 4, pp 517–519, December 1983.

[3] J.G. Maloney, G.S. Smith, and W.R. Scott, "Accurate computation of the radiation from simple antennas using the Finite-Difference Time-Domain method", *IEEE Transactions on Antennas and Propagation*, vol 38, no 7, pp 1059–1068, July 1990.

[4] G.S. Smith, *An Introduction to Electromagnetic Radiation*, Cambridge University Press, 1997, pp 599–600.

[5] P.M. Kwinana and J.H. Cloete, "Reactance of electrically short radio frequency probes", *Proc. IEEE Africon 2002*, vol 2, October 2002, pp 549–555.

Appendix B

[6] FEKO User's Manual, Suite 4.0, EM Software and Systems, Stellenbosch, South Africa, Dec 2002.

Principal Author: Phumezo Mzoxolo Kwinana holds an MSc in physics from the University of Fort Hare where he is a physics lecturer. He is currently doing PhD in Engineering Science at the University of Stellenbosch. He is financially supported by the NRF, the University of Fort Hare, and the University of Stellenbosch.

Coauthor: Johannes Hendrik Cloete is a graduate from the Universities of Stellenbosch (BSc, BEng, PhD) and California, Berkeley (MSEE). Between 1969 and 1983 he did spells in the South African Navy; the National Institute for Defence Research, Pretoria; Scientific-Atlanta Inc, Atlanta, Georgia; and the University of Pretoria. Since 1984 he has been a professor in electrical and electronic engineering at the University of Stellenbosch. He works on electromagnetic wave phenomena in stratified, dispersive matter; properties of matter at radio and microwave frequencies; and antenna design. For the past five years he has collaborated with South African and Australian engineers and scientists to introduce long-range borehole-radar technology into the South African mining industry for delineation and imaging of ore bodies and fault structures.

Appendix C

C. Measurement Results of the Electrically Short Monopoles Using HP 8510C Network Analyser

Table C-1 Measurement results for the flush monopole using HP 8510C Network Analyser

Length of the 0.141 inch 50Ω semirigid coaxial line = 0.4 m, Length of the 50Ω microstrip line = 0.3 m, Diameter of the ground plane = 765 mm, Length of the cylindrical shield = 340 mm, Diameter of the cylindrical shield (NB: cylinder closed at both ends) = 196.3 mm

S_{21} null points (at quarter wave lengths)	Resonance frequency for the unshielded flush probe (MHz)	Resonance frequency for the shielded flush probe (MHz)	Resonance frequency for the short-circuited coaxial line (MHz)	Capacitance for the bare unshielded probe (pF)	S21 magnitude for the unshielded flush probe (dB)	S21 magnitude for the shielded flush probe (dB)	Complex impedance for the flush probe (Ohms) X10^6
λ/4	131.0025	131.04		0.0211	-39.1854	-39.213	0.0012-j0.0576
2λ/4			262.15				
3λ/4	393.675	393.7		0.0045	-34.2441	-34.2831	0.0070-j0.0893
4λ/4			524.9625				
5λ/4	656.431	656.57		-0.0026	-31.7936	-31.8548	0.0154-j0.0906
6λ/4			787.6625				
7λ/4	919.4	919.48		0	-30.5311	-30.5461	1.9343-j0.00
8λ/4			1050.7				
9λ/4	1182.3	1182.4		0.001	-29.0572	-29.1591	0.0572 - j0.1027
10λ/4			1313.7				
11λ/4	1445.3	1445.3		-0.0022	-28.6394	-28.7193	0.0083 + j0.0486
12λ/4			1576.6				
13λ/4	1708.3	1708.3		0.0019	-27.6178	-27.7031	0.0095 - j0.0471
14λ/4			1839.8				
15λ/4	1971.2	1971.3		0.0052	-26.869	-26.932	0.0008 - j0.0155
16λ/4			2102.9				
17λ/4	2234.3	2234.5		0.0027	-26.7301	-26.3712	-0.0108 - j0.0208
18λ/4			2365.9				
19λ/4	2497.3	2497.3		0.0053	-25.368	-25.358	-0.0001 - j0.0120
20λ/4			2629.1				
21λ/4	2760.5	2760.5		0.0019	-25.9468	-25.9258	-0.0151 - j0.0140
22λ/4			2892.1				

Table C-2 Measurement results for the 2.5 mm monopole using HP 8510C Network Analyser

Length of the 0.141 inch 50Ω semirigid coaxial line = 0.4 m, Length of the 50Ω microstrip line = 0.3 m, Diameter of the ground plane = 765 mm, Length of the cylindrical shield = 340 mm, Diameter of the cylindrical shield (NB: cylinder closed at both ends) = 196.3 mm

S_{21} nulls (at quarter wave lengths)	Resonance frequency for the unshielded (left) & shielded (right) bare probes (MHz)		Resonance frequency for the short-circuited coaxial line (MHz)	Capacitance for the bare unshielded probe (pF)	S21 magnitude for the unshielded bare probe (dB)	S21 magnitude for the shielded bare probe (dB)	Complex impedance for bare probe (Ohms) $X10^4$
λ/4	130.71	130.77		0.1080	-39.1772	-39.2285	0.0083 -j 1.1274
2λ/4			262.15				
3λ/4	392.81	392.95		0.0884	-34.2713	-34.2996	0.0013 -j 0.4583
4λ/4			524.9625				
5λ/4	655.11	655.26		0.0742	-31.8172	-31.8439	0.0009 -j 0.3274
6λ/4			787.6625				
7λ/4	917.3875	917.77		0.0820	-30.5451	-30.5606	0.00 - j0.2116
8λ/4			1050.7				
9λ/4	1179.8	1179.7		0.0816	-29.112	-29.1728	0.0007 - j0.1653
10λ/4			1313.7				
11λ/4	1442.2	1442.5		0.0807	-28.7572	-28.6088	-0.0012 -j 0.1367
12λ/4			1576.6				
13λ/4	1704.5	1704.9		0.0867	-27.6779	-27.6819	0.0000 - j0.1077
14λ/4			1839.8				
15λ/4	1967.1	1967.4		0.0845	-26.868	-26.8984	0.0001 - j0.0957
16λ/4			2102.9				
17λ/4	2229.6	2229.6		0.0829	-26.5475	-26.3079	-0.0010 -j 0.0861
18λ/4			2365.9				
19λ/4	2492.2	2492.6		0.0825	-25.5712	-25.5385	-0.0001 -j 0.0774
20λ/4			2629.1				
21λ/4	2754.8	2755.6		0.0806	-25.5744	-25.3591	-0.0001 -j 0.0717
22λ/4			2892.1				

Table C-3 Measurement results for the 10 mm monopole using HP 8510C Network Analyser

Length of the 0.141 inch 50Ω semirigid coaxial line = 0.4 m, Length of the 50Ω microstrip line = 0.3 m, Diameter of the ground plane = 765 mm, Length of the cylindrical shield = 340 mm, Diameter of the cylindrical shield (NB: cylinder closed at both ends) = 196.3 mm

S_{21} nulls (at quarter wave lengths)	Resonance frequency for the unshielded (left) & shielded (right) bare probes (MHz)		Resonance frequency for the unshielded (left) & shielded (right) insulated probes (MHz)		Resonance frequency for the short-circuited coaxial line (MHz)	Capacitance for bare (left) & insulated (right) unshielded probes (pF)		S21 magnitude for the unshielded (left) and shielded (right) bare probes (dB)		S21 magnitude for the unshielded (left) and shielded (right) insulated probes (dB)		Complex impedance for bare (left) and insulated (right) probes (Ohms) X10^3	
λ/4	130.1875	130.1625	129.906	129.9375		0.26	0.343	-39.1441	-39.1518	-39.1408	-39.1267	0.0022 -j 4.7019	-0.0023 - j3.5698
2λ/4					262.15								
3λ/4	391.1762	391.2562	390.3975	390.4688		0.248	0.324	-34.2508	-34.2519	-34.2239	-34.2442	0.0001 -j1.6412	0.0007 - j1.2567
4λ/4					524.9625								
5λ/4	652.412	652.288	651.075	651.075		0.232	0.311	-31.8087	-31.8368	-31.8099	-31.8237	0.0009 - j1.0520	0.0003 - j0.7868
6λ/4					787.6625								
7λ/4	913.74	913.76	911.78	911.82		0.234	0.317	-30.5115	-30.5339	-30.4888	-30.5069	0.0004 - j0.7434	0.0002 - j0.5513
8λ/4					1050.7								
9λ/4	1174.8	1174.5	1172.4	1172.1		0.244	0.322	-29.0706	-28.9622	-29.0109	-28.9689	-0.0014 - j0.555	-0.0003 - j0.4211
10λ/4					1313.7								
11λ/4	1436.0	1436.1	1433.0	1433.285		0.244	0.324	-28.4747	-28.5334	-28.3542	-28.5185	0.0005 -j 0.4537	0.0008 -j 0.3424
12λ/4					1576.6								
13λ/4	1697.2	1697.3	1693.3	1693.4		0.251	0.339	-27.4264	-27.6349	-27.3013	-27.6358	0.0014 -j 0.3739	0.0013 - j0.2773
14λ/4					1839.8								
15λ/4	1958.3	1958.4	1953.9	1953.9		0.256	0.342	-26.5973	-26.8492	-26.4152	-27.7980	0.0014 -j 0.3177	0.0040 -j 0.2380
16λ/4					2102.9								
17λ/4	2219.5	2219.4	2214.4	2206.9		0.256	0.3446	-25.91	-26.2074	-25.5479	-26.2493	0.0013 -j 0.2797	0.0018 - j0.2086
18λ/4					2365.9								
19λ/4	2480.1	2479.7	2474.1	2473.3		0.269	0.362	-24.519	-25.5123	-23.9545	-25.4891	0.0038 -j 0.2384	0.0033 - j0.1776
20λ/4					2629.1								
21λ/4	2741.1	2740.4	2733.9	2734.5		0.271	0.372	-24.0824	-25.1288	-23.1928	-25.0089	0.0046 -j 0.2141	0.0032 - j0.1564
22λ/4					2892.1								

Table C-4 Measurement results for the 20 mm probe using HP 8510C Network Analyser

Length of the 0.141 inch 50Ω semirigid coaxial line = 0.4 m, Length of the 50Ω microstrip line = 0.3 m, Diameter of the ground plane = 765 mm, Length of the cylindrical shield = 340 mm, Diameter of the cylindrical shield (NB: cylinder closed at both ends) = 196.3 mm

S_{21} nulls (at quarter wave lengths)	Resonance frequency for the unshielded (left) & shielded (right) bare probes (MHz)		Resonance frequency for the unshielded (left) & shielded (right) insulated probes (MHz)		Resonance frequency for the short-circuited coaxial line (MHz)	Capacitance for the bare (left) & insulated (right) unshielded probes (pF)		S21 magnitude for the unshielded (left) and shielded (right) bare probes (dB)		S21 magnitude for the unshielded (left) and shielded (right) insulated probes (dB)		Complex impedance for bare (left) and insulated (right) probes (Ohms) $X10^3$	
λ/4	129.725	129.656	129.3	129.325		0.3970	0.5237	-39.0918	-39.1489	-39.1278	-39.1985	0.0070 - j3.0903	0.0050 - j2.3504
2λ/4					262.15								
3λ/4	389.71	389.71	388.56	388.56		0.3922	0.5061	-34.1969	-34.2701	-34.1964	-34.2407	0.0018 -j1.0413	0.0007 - j0.8093
4λ/4					524.9625								
5λ/4	649.75	649.82	648.11	647.866		0.3890	0.4863	-31.71	-31.8131	-31.6503	-31.7839	0.0012 -j 0.6297	0.0010 -j 0.5050
6λ/4					787.6625								
7λ/4	909.81	909.69	906.9	906.69		0.3997	0.5232	-30.2586	-30.5019	-30.0918	-30.4894	0.0016 -j 0.4377	0.0016 - j0.3354
8λ/4					1050.7								
9λ/4	1169.3	1167.2	1165.6	1162.9		0.4241	0.5463	-28.4522	-28.837	-28.0099	-28.8361	0.0017 -j 0.3209	0.0023 –j 0.2499
10λ/4					1313.7								
11λ/4	1428.6	1428.3	1423.4	1423.2		0.4427	0.5833	-27.2621	-28.4906	-26.4249	-28.4101	0.0036 -j 0.2516	0.0036 -j 0.1916
12λ/4					1576.6								
13λ/4	1687.0	1687.2	1679.9	1680.4		0.4823	0.6452	-25.1204	-227.603	-23.7765	-27.5213	0.0053 -j 0.1955	0.0049 – j 0.1467
14λ/4					1839.8								
15λ/4	1944.5	1945.0	1934.9	1935.8		0.5276	0.7190	-22.2522	-26.7373	-20.0485	-26.6591	0.0075 - j0.1548	0.0069 -j 0.1140
16λ/4					2102.9								
17λ/4	2200.7	2200.6	2187.8	2187.6		0.5836	0.8113	-19.9599	-26.6152	-16.9941	-25.96	0.0085 - j0.1233	0.0073 – j 0.0891
18λ/4					2365.9								
19λ/4	2454.6	2445.8	2436.8	2423.1		0.6670	0.9497	-15.0842	-25.2732	-11.6009	-24.9891	0.0121 - j0.0957	0.0093 – j 0.0675
20λ/4					2629.1								

Table C-5 Measurement results for the 40 mm monopole using HP 8510C Network Analyser

Length of the 0.141 inch 50Ω semirigid coaxial line = 0.4 m, Length of the 50Ω microstrip line = 0.3 m, Diameter of the ground plane = 765 mm, Length of the cylindrical shield = 340 mm, Diameter of the cylindrical shield (NB: cylinder closed at both ends) = 196.3 mm

S_{21} nulls (at quarter wave lengths)	Resonance frequency for the unshielded (left) & shielded (right) bare probes (MHz)		Resonance frequency for the unshielded (left) & shielded (right) insulated probes (MHz)		Resonance frequency for the short-circuited coaxial line (MHz)	Capacitance for the bare (left) & insulated (right) unshielded probes (pF)		S21 magnitude for the unshielded (left) and shielded (right) bare probes (dB)		S21 magnitude for the unshielded (left) and shielded (right) insulated probes (dB)		Complex impedance for bare (left) and insulated (right) probes (Ohms) $X10^3$	
λ/4	128.844	128.84	128.325	128.35		0.6606	0.8175	-39.1007	-39.1307	-39.1134	-39.1658	0.0013 - j1.8699	0.0015 - j1.5171
2λ/4					262.15								
3λ/4	386.99	387.0125	385.43	385.4375		0.6627	0.8196	-34.0696	-34.2418	-33.9862	-34.2120	0.0015 -j 0.6206	0.0013 - j0.5038
4λ/4					524.9625								
5λ/4	644.41	644.35	641.4675	641.52		0.7079	0.8858	-31.0804	-31.7783	-30.7719	-31.7383	0.0026 - j0.3489	0.0024 - j0.2801
6λ/4					787.6625								
7λ/4	900.23	899.575	895.194	894.156		0.8090	1.0278	-27.2907	-30.4185	-25.9102	-30.3242	0.0063 -j 0.2184	0.0061 -j 0.1728
8λ/4					1050.7								
9λ/4	1152.0	1131.2	1142.2	1115.5		0.9953	1.3372	-21.0077	-27.66	-18.3538	-27.6237	0.0091 -j 0.1382	0.0083 -j 0.1035
10λ/4					1313.7								

Appendix D

Appendix D-1

Experimental determination of the attenuation constant of the coaxial and microstrip lines

The attenuations of both the coaxial and microstrip lines were experimentally determined by the measurement of transmission coefficients using the HP 8510C network analyser. The network analyser was carefully calibrated using high quality calibration kit. The 0.141 inch semi rigid coaxial line, 0.345 ± 0.02 m long, was designed with the female SMA connectors at both ends. Also, the 0.3m long 50Ω microstrip line was designed with the female SMA connectors at both ends. From the transmission line theory, it can be shown that the transmission coefficient is given by [15]:

$$S_{21} = e^{-\alpha L} e^{-j\beta L} \qquad \text{(D-1)}$$

Where L is the length of the coaxial line, α, the attenuation constant, and β the phase constant. The magnitude is therefore given by:

$$|S_{21}| = e^{-\alpha L} \qquad \text{(D-2)}$$

On rearranging equation D-2, it can be shown that the equation for computing attenuation from the measured data is given by:

$$\text{Attenuation} = (8.686/L)\text{Log}|S_{21}| \text{ dB/m} \qquad \text{(D-3)}$$

The attenuation of the microstrip was similarly determined. Transmission coefficient measurements of both the coaxial and the microstrip lines were taken in the frequency range from 45 MHz to 2 GHz. The graphical representation of the experimental results is given below. From Fig. D-1, it can be seen that the attenuation of the coaxial line is slightly below that of the microstrip line. This is due to the fact that the fields in the coaxial line are confined compared to those of the microstrip line. The

attenuation of the coaxial line at 500 MHz agrees with the published data [Appendix A] by 20%.

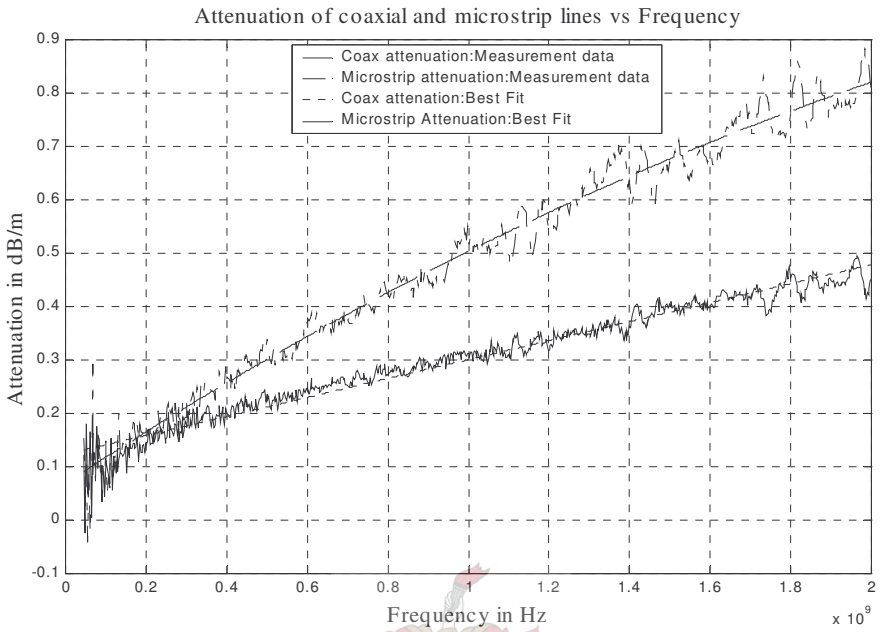

Fig. D-1 Results of attenuation for coaxial and microstrip lines

Appendix D-2

Experimental determination of the characteristic impedance of the coaxial and microstrip lines.

The characteristic impedances of both the coaxial and microstrip lines were experimentally determined by the measurement of their input impedances at quarter-wave multiples using the HP 8510C network analyser. The network analyser was carefully calibrated using high quality calibration kit. The 0.141 inch semi rigid coaxial line, 0.345 ± 0.02 m long, with the female SMA connectors at both ends and the 0.3m long 50Ω microstrip line with the female SMA connectors at both ends were again used for this experiment.

From the transmission line theory, the quarter-wave impedance for low-loss lines is given by [15, Chapter 5, Table 5.11a]:

$$Z_{in} = Z_0\left[\frac{Z_0 + Z_L \alpha L}{Z_L + Z_0 \alpha L}\right] \qquad \text{(D-4)}$$

Where Z_{in} is the input impedance at each quarter-wave multiple of the line, Z_0 the characteristic impedance, Z_L the load impedance, L the length of the line, and α the attenuation constant. On rearranging equation D-4 and making Z_0 the subject of the formula, the expression for the characteristic impedance is given by:

$$Z_0 = ((\alpha L)/2)(Z_{in} - Z_L) \pm \sqrt{((\alpha L)/2)^2 (Z_L - Z_{in})^2 + Z_{in} Z_L} \qquad \text{(D-5)}$$

Both lines were terminated with the 110Ω resistors. Attenuation and input impedance were obtained at each quarter-wave multiple. The results are presented on the graph below:

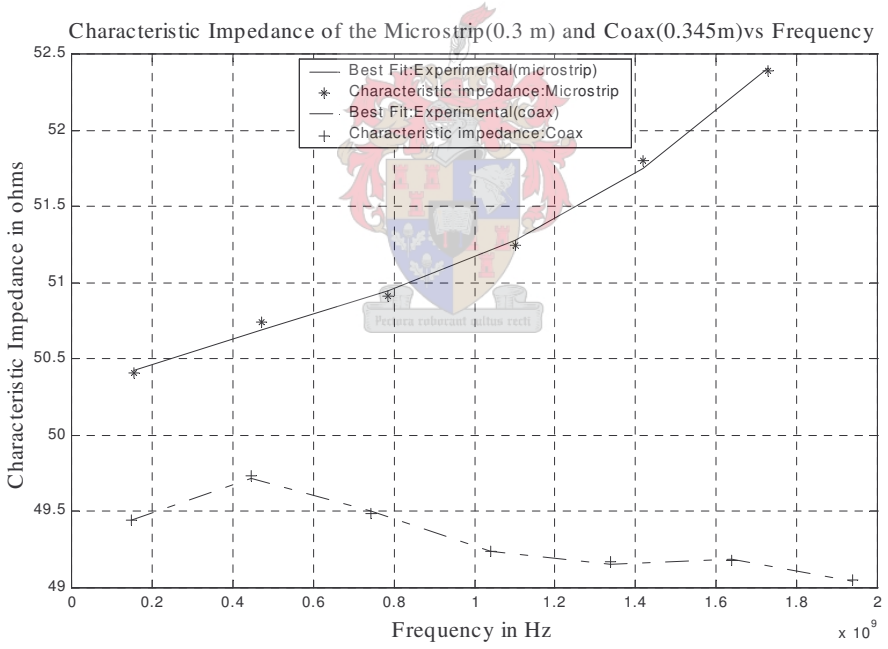

Fig. D-2 Measurement results of characteristic impedance for coaxial and microstrip lines

From Fig.D-2, it can be seen that the maximum deviation of the measured characteristic impedances to 50Ω is about 5% and 2% for microstrip and the coaxial line respectively. The graph for the microstrip characteristic impedance is slightly sloping up as the frequency increases. This is due to the discontinuity of the transition from the SMA connector to the microstrip line which is the different type of transmission line as the coaxial line.